The Achievable Rate Region of 802.11-Scheduled Multihop Networks

Apoorva Jindal, *Member, IEEE*, and Konstantinos Psounis, *Senior Member, IEEE*

***Abstract*—In this paper, we characterize the achievable rate region for any IEEE 802.11-scheduled static multihop network. To do so, we first characterize the achievable edge-rate region, that is, the set of edge rates that are achievable on the given topology. This requires a careful consideration of the interdependence among edges since neighboring edges collide with and affect the idle time perceived by the edge under study. We approach this problem in two steps. First, we consider two-edge topologies and study the fundamental ways they interact. Then, we consider arbitrary multihop topologies, compute the effect that each neighboring edge has on the edge under study in isolation, and combine to get the aggregate effect. We then use the characterization of the achievable edge-rate region to characterize the achievable rate region. We verify the accuracy of our analysis by comparing the achievable rate region derived from simulations with the one derived analytically. We make a couple of interesting and somewhat surprising observations while deriving the rate regions. First, the achievable rate region with 802.11 scheduling is not necessarily convex. Second, the performance of 802.11 is surprisingly good. For example, in all the topologies used for model verification, the max-min allocation under 802.11 is at least 64% of the max-min allocation under a perfect scheduler.**

***Index Terms*—Capacity region, IEEE 802.11, multihop networks.**

I. Introduction

A CENTRAL question in the study of multihop networks is the following: Given an arbitrary multihop topology and a collection of source–destination pairs, what is the achievable rate region of this arbitrary multihop network? Researchers have formulated a multicommodity flow problem to answer this question [1], [2]. These papers assume optimal scheduling with different interference models at the MAC layer in their formulations. However, the MAC protocol used in all the multihop networks being deployed is IEEE 802.11 (see, for example, [3]–[6]). Characterizing the achievable rate region of an arbitrary multihop network with 802.11 scheduling is still an open problem and is the focus of this work. This characterization will have several applications. For example, it will allow researchers who propose new rate control or routing protocols for multihop networks with 802.11 scheduling to compare the performance of their scheme with the optimal value.

Setting up a multicommodity flow formulation for 802.11-scheduled multihop networks runs into the following problem: What is the *achievable edge-rate region* of the given multihop topology? The achievable edge-rate region is the region characterizing the set of *edge rates* achievable on the given multihop topology. For example, for a wireline network, this region is simply characterized by the constraint that the sum of flow rates at each edge is less than the data rate of the edge. For a multihop network with optimal scheduling, this region is characterized using independent sets [1]. Characterizing this region is the main missing step in the characterization of the achievable rate region for 802.11-scheduled multihop networks.

Related Work: There is a large body of interesting work on modeling the behavior of IEEE 802.11 in a multihop network. This work can be subdivided into five broad categories. 1) [7] and [8] present a detailed analysis for specific topologies under study (like the flow in the middle topology or the chain topology), but their methodology cannot be applied to any arbitrary topology. 2) [9]–[11] propose a methodology independent of the topology at hand, but in order to keep the analysis tractable, they simplify the operation of the 802.11 protocol. In particular, they ignore lack-of-coordination problems due to topology asymmetries and/or certain aspects of the protocol like the binary exponential backoff mechanism. 3) [12]–[14] focus on modeling and analyzing interference at the physical layer. To eliminate MAC issues that complicate the analysis without affecting the physical layer model, they assume that all transmitters are within range of each other and ignore certain aspects of the 802.11 protocol like the binary exponential backoff mechanism and ACK packets. Our work is complementary to papers of this category. We use a simplified physical layer model but a complete model for 802.11 MAC layer with no assumption on the topology at hand. Please refer to [23] for a discussion on how to extend the MAC layer analysis presented in this paper to the more sophisticated physical layer models proposed by papers of this category. 4) [15]–[17] are perhaps the closest to our work. They present a general methodology without making any simplifications to the 802.11 protocol. However, their methodology cannot be applied to topologies that have nodes with multiple outgoing edges, and hence, cannot be used to study any arbitrary multihop topology. Furthermore, these papers do not incorporate all the possible dependencies which can exist between both neighboring and nonneighboring edges, which makes them increasingly inaccurate as the packet transmission time increases. 5) [18] proposed a complete model to derive the one-hop throughput for 802.11 in multihop topologies. This model is more accurate than the previous ones because it uses a Markov chain to capture the complete network state in each of its states. However, the Markov chain has an exponential number of states that precludes the model's use for any decent-sized network. (For example, a typical 20-node network will require constructing and solving a Markov chain with more than 500 000 states.) To summarize, an accurate,

Manuscript received April 21, 2008; revised September 09, 2008; approved by IEEE/ACM TRANSACTIONS ON NETWORKING Editor S. Kalyaranaman. First published May 27, 2009; current version published August 19, 2009.

The authors are with the Department of Electrical Engineering, University of Southern California, Los Angeles, CA 90089 USA (e-mail: apoorvaj@usc.edu; kpsounis@usc.edu).

Color versions of one or more of the figures in this paper are available online at http://ieeexplore.ieee.org.

Digital Object Identifier 10.1109/TNET.2008.2007844

general, and scalable method to characterize the achievable edge-rate region for an 802.11-scheduled multihop network is still missing.

Our Contributions: The main contribution of this work is to characterize the achievable edge-rate region for any given multihop topology in a scalable manner. We adopt the following methodology to characterize this region. We first find the expected service time at a particular edge in terms of the collision probability at the receiver and the idle time perceived by the transmitter of that edge. The hard part in the procedure is to find these collision probabilities and idle times because their value depends on the edge-rates at other edges in the network. To find the value of these variables, we decompose the local network topology into a number of two-edge topologies, derive the value of these variables for these two-edge topologies, and then appropriately combine them. Finding the expected service time at each edge allows us to characterize the achievable edge-rate region. It is important to note that this "decompose-and-combine" approach that we follow provides an intuitive, precise description of *how neighboring nodes of a multihop wireless network affect each other under a random scheduler like 802.11*.

We use the characterization of the achievable edge-rate region to characterize the achievable flow-rate region[1] for any multihop network and a collection of source–destination pairs. We then verify the accuracy of our analysis by comparing the achievable flow-rate region derived by simulations to the one derived by analysis for different topologies. We make a couple of interesting observations from these achievable flow-rate regions. First, the achievable flow-rate region for an 802.11-scheduled multihop network is not necessarily convex. Second, for all the topologies studied in this paper, the max-min rate allocation under 802.11 is at least 64% of the max-min allocation under a perfect scheduler.

The outline of the rest of this paper is as follows. First, we introduce the network model and the simulation setup in Section II. Then, Sections III and IV describe the methodology to characterize the achievable edge-rate and flow-rate region, respectively, for any multihop topology and a collection of source–destination pairs. Section V verifies the accuracy of the model by comparing achievable rate regions derived theoretically and via simulations. Section VI discusses some approximations that allow to solve the coupled system of multivariate equations derived in Section III without an iterative procedure. Finally, Section VII concludes and discusses some future directions.

II. Preliminaries

A. Network Model

We assume that the static multihop topology is given as an input. An edge between two nodes implies that the two nodes interfere with each other (irrespective of whether they can hear each other's transmission successfully). Thus, the input topology is defined by the interference graph $\mathcal{G} = (V, E)$, where V is the set of all nodes and E is the set of all edges. The interference is assumed to be binary—i.e., a transmission emanating from one of these interfering nodes will always cause a collision at the other node—and pairwise, i.e., interference happens between these node pairs only. This interference model neglects some physical-layer issues like the capture effect [13] and the effect of multiple interferers [19]. However, to understand the behavior of the 802.11 MAC and derive the achievable rate region associated with 802.11 MAC layer without making any simplifications in the protocol, we purposely neglect these physical-layer issues. Their absence is not altering critical MAC properties, while their inclusion would unnecessarily complicate the analysis. [23] discusses how to remove the binary and pairwise assumptions on interference.

[1]Achievable flow-rate region is also referred to as the achievable rate region. Both these terms are used interchangeably in this paper.

TABLE I
Brief Description of the Notation Used in the Analysis (Refer to the Text for Precise Definitions)

T_e	Transmitter of e
R_e	Receiver of e
λ_e	Edge rate at e
$E[S_e]$	Expected service time at e
p^e_{RTS} (p^e_{CTS} p^e_{DATA}, p^e_{ACK})	Probability of successful RTS (CTS, DATA, ACK) transmission in absence of collisions
T_s	Time taken to complete one packet transmission
T_c	Time wasted in an RTS collision
$p^{e,T}_{c,i}$	Probability of successful RTS-CTS exchange when backoff window value at T_e is W_i
$p^{e,T}_{l,i}$	Probability of successful DATA-ACK exchange when backoff window value at T_e is W_i
$p^{e,T}_{idle}$	Probability that channel is idle around T_e
$p^e_{w_0}$	Probability that the backoff counter at e is equal to 0
$K_{e,T}$	Expected number of DATA transmissions per packet
N^e	Set of edges which interfere with e

In the absence of a collision, a transmission may get lost due to physical-layer imperfections like fading, hardware noise, etc. Successful reception of the RTS, CTS, DATA, and ACK packets transmitted on some edge $e \in E$ in absence of collisions are modeled as Bernoulli random variables with success probability equal to p^e_{RTS}, p^e_{CTS}, p^e_{DATA}, and p^e_{ACK}, respectively. (Note that if two nodes are within each other's interference range but outside each other's transmission range, then these probabilities are equal to 0.) Table I summarizes the notation introduced in this (and the next) section.

We assume that the set of flows $\mathcal{F}$ is also given as an input. Each flow $f \in \mathcal{F}$ is represented by a source–destination pair. Let $s(f)$ denote the source and $d(f)$ denote the destination for flow f. We assume that the arrival process for each flow f has i.i.d. (independent and identically distributed) interarrival times and a long-term rate equal to r_f. We also assume independence between the arrival process for different flows[2] and denote the edge rate (sum of the flow rates at the edge) induced by these flows on edge e by λ_e. A given set of edge rates $\Lambda_E = \{\lambda_e : e \in E\}$ is said to be achievable if the input rate at each queue in the network is less than the service rate at that queue. Then, a given set of end-to-end flow rates is said to be achievable if there exists a routing (multiple paths per flow are possible) such that the induced set of edge rates is achievable. The achievable edge-rate and flow-rate regions are then defined as the closures of the corresponding achievable sets of rates.

We assume that each node is running IEEE 802.11 with RTS/CTS at the MAC layer. (We assume RTS/CTS because its use is suggested by the 802.11 standard, and we do not want to ignore any part of the protocol.) Let W_0 and m denote the initial backoff window and the number of exponential backoff

[2]Since we assume independent interarrival times and independence between the arrival process for different flows, what we derive is a lower bound on the capacity region derived without any assumption on the arrival processes.

TABLE II
SYSTEM PARAMETERS USED TO OBTAIN NUMERICAL RESULTS

Packet Payload	1024
MAC Header	34 bytes
PHY Header	16 bytes
ACK	14 bytes + PHY header
RTS	20 bytes + PHY header
CTS	14 bytes + PHY header
Channel Bit Rate	1 Mbps
Propagation Delay	1 μs
Slot Time	20 μs
SIFS	10 μs
DIFS	50 μs
W_0	31
m	5

windows, respectively. We assume that the basic time unit is equal to one backoff slot time. Let T_{RTS}, T_{CTS}, T_{DATA}, and T_{ACK} denote the time taken to transmit one RTS, CTS, DATA, and ACK packet, respectively. (Note that the DATA packet includes the UDP, IP, MAC, and PHY headers along with the payload.) We also assume that all packets are of the same size, so T_{DATA} is a constant. Let T_c denote the time wasted in an RTS collision and let T_s denote the time it takes to complete one packet transmission. Then, $T_c = T_{\mathrm{RTS}} + \mathrm{DIFS} + \delta$ and $T_s = T_{\mathrm{RTS}} + \mathrm{SIFS} + \delta + T_{\mathrm{CTS}} + \mathrm{SIFS} + \delta + T_{\mathrm{DATA}} + \mathrm{SIFS} + \delta + T_{\mathrm{ACK}} + \mathrm{DIFS} + \delta$, where δ is the propagation delay and DIFS and SIFS are IEEE 802.11 parameters.[3]

We will be making the following two assumptions throughout the paper to simplify the analysis.

Assumption 1: First, we assume $T_{\mathrm{RTS}} \ll T_s$ and $T_{\mathrm{CTS}} \ll T_s$. The protocol description recommends the use of RTS/CTS only when the size of the DATA packet is much larger than the size of the RTS packets. This is in line with the fundamental principle that the load due to control packets should be a small fraction of the total load. Hence, this assumption is satisfied for normal protocol operation.

Assumption 2: Second, we assume that $W_0 \gg 1$. Default 802.11 parameters satisfy this assumption. In general, choosing a small value for W_0 will not properly regulate random access to the channel and will cause a lot of collisions and throughput loss even for WLANs. Hence, this assumption is also satisfied for normal protocol operation.

B. Simulation Setup

We use simulations to verify the accuracy of our analysis. We use Qualnet 4.0 as the simulation platform in this paper. All our simulations are conducted using an unmodified 802.11(b) MAC (DCF) with RTS/CTS. We use default parameters of 802.11(b) (summarized in Table II) in Qualnet unless otherwise stated. Auto-rate adaptation at the MAC layer is turned off, and the rate is fixed at 1 Mbps. We set the buffer size and maximum retry limit in 802.11 (the number of retransmission attempts after which the packet is dropped) to a very large value to avoid packet losses. This allows us to generate the achievable rate region without having to worry about transport-layer retransmissions to recover from these losses. The packet size is fixed to be 1024 bytes. To use simulations to validate the theoretically derived capacity region, we simulate all possible combinations of flow rates, with each flow rate varying from 0 to 1 Mbps in steps of 10 Kbps, and plot the achieved output rate at the destination.

[3]We do not provide a description of IEEE 802.11 protocol. Please refer to [20] for a detailed description of the protocol.

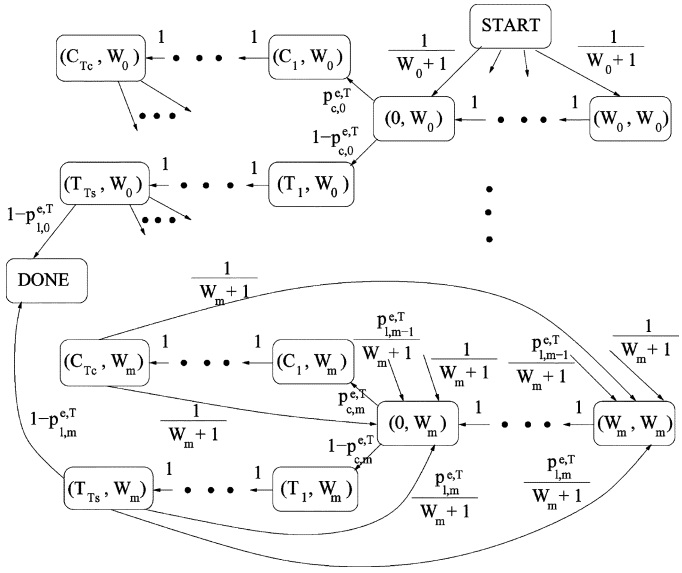

Fig. 1. The Markov chain representing the evolution of a transmitter's state.

III. CHARACTERIZING THE ACHIEVABLE EDGE-RATE REGION

This section characterizes the achievable edge-rate region Λ_E for any multihop topology.

A. Expected Service Time of an Edge

This section finds the expected service time of a particular edge (denoted by e) in a particular topology (denoted by T) by constructing and solving a Markov chain (MC) for this edge. The states of this MC describe the current backoff window, backoff counter, and time since the last successful/unsuccessful RTS/CTS exchange (see next paragraph for details). The transition probabilities of this MC for e depend on the collision probabilities at the receiver of e, which, in turn, depend on the exact state at the other edges in the network. In order to decouple the MCs and reduce the state space, we find the average value of the collision probabilities by averaging over all possible events, which can cause a collision at the receiver. (Note that these events are not independent.) The dependence between the different edges, and consequently MCs, is captured via these average probabilities.

Prior work on the analysis of 802.11 has also attempted to reduce the state space of a MC describing the backoff window and counter values. For single-hop networks, the author in [21] assumed node homogeneity and independence, an approach which has been justified rigorously recently [22]. In the context of multihop networks [15], [17] a somewhat similar approach to ours has been used, but not all events leading to collisions have been considered, and these events have been assumed to be independent. Later sections describe how to find the value of these average collision probabilities. Here, we focus on finding the expected service time, assuming these probabilities are given.

The evolution of the 802.11 MAC layer state at the transmitter of edge e after receiving a packet from the network layer is represented by the absorbing MC shown in Fig. 1. The MC starts from the state *START* (which represents a packet entering the MAC layer to be scheduled for transmission) and ends in the state *DONE* (which represents the end of a successful packet transmission). The expected service time at e is equal to the expected time it takes for the MC to reach *DONE* from *START*.

The state (j, W_i), $0 \le j \le W_i$, $0 \le i \le m$, represents the transmitter state, where the backoff window is equal to W_i and the backoff counter is equal to j. The backoff counter keeps decrementing until it expires (reaches state $(0, W_i)$), which is then followed by a transmission attempt. The transmitter first attempts an RTS–CTS exchange, which fails with probability $p_{c,i}^{e,T}$. (Thus, $p_{c,i}^{e,T}$ denotes the probability that the RTS–CTS exchange at edge e in topology T is unsuccessful given that either the RTS/CTS exchange or the DATA/ACK exchange was unsuccessful in the previous i transmission attempts.) Note that Table I contains a brief summary of the variables that are being rigorously defined in this section. The states (C_k, W_i), $1 \le k \le T_c$, represent an unsuccessful RTS/CTS exchange k time-units before, while the states (T_k, W_i), $1 \le k \le T_s$, represent a successful RTS–CTS exchange k time-units before, followed by the DATA–ACK exchange that fails with probability $p_{l,i}^{e,T}$. (Thus, $p_{l,i}^{e,T}$ denotes the probability that the DATA–ACK exchange is unsuccessful given that the RTS–CTS exchange was successful, and either the RTS/CTS exchange or the DATA/ACK exchange was unsuccessful in the previous i transmission attempts.) If the DATA–ACK exchange is successful, the MC moves to the state *DONE*. If either the RTS/CTS or the DATA/ACK exchange is unsuccessful, then the backoff window is set to W_{i+1} if $i < m$, and to W_m if $i = m$, the backoff counter is chosen uniformly at random in between 0 and the new backoff window value, and the MC jumps to the corresponding state.

Note that $p_{c,i}^{e,T}$ and $p_{l,i}^{e,T}$ depend on i, which denotes the number of successive transmission failures. Since the probability that there are more than $m+1$ successive transmission failures is small for the default values of 802.11, we approximate $p_{c,i}^{e,T}$ and $p_{l,i}^{e,T}$ for $i > m$ by $p_{c,m}^{e,T}$ and $p_{l,m}^{e,T}$. In case one decides to not use the default parameters of 802.11 and set m to a smaller value, then one can introduce additional states in the MC until some value $m' > m$ such that the probability of $m'+1$ successive transmission failures is small.

This MC does not capture the duration of time the backoff counter may get frozen due to another transmission within the transmitter's neighborhood (due to the physical/virtual carrier sensing mechanism of the 802.11 protocol). To capture this, let $p_{\text{idle}}^{e,T}$ denote the proportion of time the channel around the transmitter of edge e is idle conditioned on the event that there is no successful transmission ongoing at e. We now use the MC to derive the expected service time at edge e (denoted by $E[S_e]$) in (1) in terms of the collision and idle probabilities. For ease of presentation, we define the following two additional variables: Let $E[T_{W_i}^{c,e}]$ and $E[T_{W_i}^{l,e}]$ for $1 \le i \le m$ denote the additional time required to reach the start of a successful packet transmission given that the backoff window just got incremented to W_i due to an unsuccessful RTS–CTS and DATA–ACK exchange, respectively.

$$\begin{aligned} E\left[T_{W_i}^{c,e}\right] &= T_c + \frac{W_i+1}{2p_{\text{idle}}^{e,T}} + p_{c,i}^{e,T} E\left[T_{W_{n_i}}^{c,e}\right] \\ &\quad + \left(1 - p_{c,i}^{e,T}\right) p_{l,i}^{e,T} E\left[T_{W_{n_i}}^{l,e}\right] \\ E\left[T_{W_i}^{l,e}\right] &= T_s + \frac{W_i+1}{2p_{\text{idle}}^{e,T}} + p_{c,i}^{e,T} E\left[T_{W_{n_i}}^{c,e}\right] \\ &\quad + \left(1 - p_{c,i}^{e,T}\right) p_{l,i}^{e,T} E\left[T_{W_{n_i}}^{l,e}\right] \end{aligned}$$

$$\begin{aligned} E[S_e] &= T_s + \frac{W_0+1}{2p_{\text{idle}}^{e,T}} + p_{c,0}^{e,T} E\left[T_{W_1}^{c,e}\right] \\ &\quad + \left(1 - p_{c,0}^{e,T}\right) p_{l,0}^{e,T} E\left[T_{W_1}^{l,e}\right] \end{aligned} \tag{1}$$

where $n_i = \begin{cases} i+1 & \text{if } 1 \le i \le m-1, \\ m & \text{if } i = m \end{cases}$. Note that (1) is derived based on the following rule for finding the mean time to reach an absorbing state in an absorbing MC: Let $\mathcal{S}$ denote all the states of a MC, let p_{ij} denote the transition probability from state i to state j, let $k \in \mathcal{S}$ denote the absorbing state, and let T_{jk} denote the mean time to reach state k from state j. Then. $T_{ik} = p_{ik} + \sum_{j \in S} p_{ij} T_{jk}$.

To derive the value of the expected service time at a particular edge e using (1), one has to first find the value of $p_{c,i}^{e,T}$, $p_{l,i}^{e,T}$, and $p_{\text{idle}}^{e,T}$ for that edge. The next two sections describe how to find the value of these variables for any edge in a given multihop topology.

Note that we have neglected the effect of post-backoff in this MC. (Post-backoff refers to backing off right after the transmission of the last packet in the queue in anticipation of a future packet for which there will be no backoff if post-backoff has completed in the meantime.) Since we are interested in determining the boundary of the capacity region, this will have a negligible impact on the accuracy. This is because the boundary of the capacity region depends on the service rate of the backlogged edges, such edges are almost always busy and do not post-backoff, and their dependence on nonbacklogged edges is nearly unaffected by the post-backoff taking place in these nonbacklogged edges.

B. Derivation of Collision and Idle Probabilities for Two-Edge Topologies

This section finds the collision and idle probabilities for all possible two-edge topologies. A two-edge topology is defined to be one that has two distinct edges not sharing the same transmitter. These two-edge topologies reveal the types of interdependence that can exist between two edges in a multihop network and an analysis for these topologies will serve as the building block for the analysis of more complex topologies, as will be seen in the next section. [15] identified four different categories of two-edge topologies that can exist in a given multihop network and analyzed them to study unfairness in 802.11 networks. Here we derive the achievable edge-rate region for these topologies. (This list is exhaustive, that is, all possible two-edge topologies belong to one of these four categories.) We use the following notation throughout this section: e_1 and e_2 denote the two edges under consideration, and λ_{e_j}, $j = 1, 2$, denotes the edge rates (in packets/time unit). Further, let T_{e_j} and R_{e_j}, $j = 1, 2$, denote the transmitter and the receiver of the two edges. Finally, let $E_{\text{RTS}}^{t,r}$ and $E_{\text{CTS}}^{t,r}$, $t, r \in \{T_{e_1}, T_{e_2}, R_{e_1}, R_{e_2}\}$, denote the event that the RTS and the CTS packet transmitted by node t is not correctly received at node r due to physical-layer errors, respectively. For example, $E_{\text{CTS}}^{R_{e_1}, T_{e_2}}$ denotes the event that the CTS transmitted by R_{e_1} is not correctly received at T_{e_2} due to physical-layer errors.

1) Coordinated Stations (CoS): A two-edge topology is a coordinated station topology if T_{e_1} and T_{e_2} interfere with each other. Fig. 2(a) shows an example of a coordinated station topology. Note that there are other two-edge topologies also where T_{e_1} and T_{e_2} interfere with each other but with no

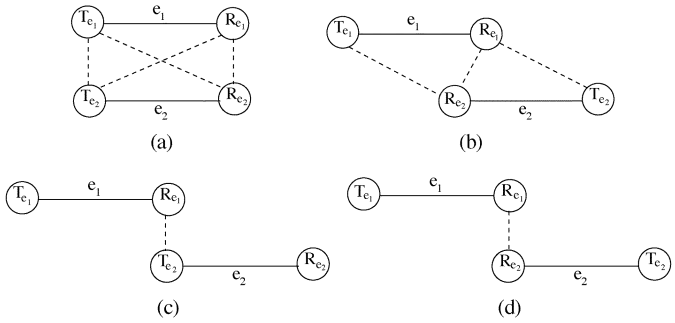

Fig. 2. Different two-edge topologies: (a) coordinated stations, (b) near hidden edges, (c) asymmetric topology, and (d) far hidden edges.

interference links between T_{e_1} and R_{e_2} and/or T_{e_2} and R_{e_1}. However, the performance profile and most of the analysis remains the same. Hence, all these topologies are referred to as coordinated stations. The minor change introduced by the lack of interference links between T_{e_1} and R_{e_2} and/or T_{e_2} and R_{e_1} is discussed at the end of this section.

We first state the value of $p_{l,i}^{e_j,\mathrm{CoS}}$ in the following lemma.

Lemma 1: $p_{l,i}^{e_j,\mathrm{CoS}} = 1 - (p_{\mathrm{DATA}}^{e_j} \times p_{\mathrm{ACK}}^{e_j})$, $0 \le i \le m$, $j = 1, 2$.

Proof: For this topology, the RTS–CTS exchange will successfully avoid any DATA collision, and the DATA–ACK exchange will be unsuccessful, only when the DATA or the ACK packet gets corrupted due to physical-layer effects. ■

We next derive the value of $p_{c,i}^{e_j,\mathrm{CoS}}$. Note that the analysis presented in [21] can be directly applied for this topology to derive the value of $p_{c,i}^{e_j,\mathrm{CoS}}$ under saturation conditions (when transmitters always have a packet to send). The following lemma finds this probability for nonsaturation conditions.

Lemma 2:

(i) $p_{c,i}^{e_1,\mathrm{CoS}} = 1 - (p_{\mathrm{RTS}}^{e_1} \times p_{\mathrm{CTS}}^{e_1}(1 - \lambda_{e_2} E[S_{e_2}] p_{w_0}^{e_2}))$, $0 \le i \le m$;

(ii) $p_{c,i}^{e_2,\mathrm{CoS}} = 1 - (p_{\mathrm{RTS}}^{e_2} \times p_{\mathrm{CTS}}^{e_2}(1 - \lambda_{e_1} E[S_{e_1}] p_{w_0}^{e_1}))$, $0 \le i \le m$

where $2/(W_m+1) \le p_{w_0}^{e} \le 2/(W_0+1)$ is the probability that the backoff counter at edge e is equal to 0.

Proof: We first look at edge e_1. The RTS/CTS exchange is unsuccessful if either the RTS or the CTS is lost due to physical-layer errors or an RTS collision happens at R_{e_1}. An RTS collision will occur only if the backoff counter at edge e_2 also expires in the same slot duration, resulting in both T_{e_1} and T_{e_2} sending an RTS packet. Thus, $p_{c,i}^{e_1,\mathrm{CoS}} = P(e_2 \text{ has a packet to send}) \times p_{w_0}^{e_2}$. a) $P(e_2 \text{ has a packet to send}) = \lambda_{e_2} E[S_{e_2}]$ as the probability that a queueing system is nonempty is equal to $\lambda E[S]$, where λ is the packet arrival rate into the system and $E[S]$ is the expected service time. b) As derived in [21], $p_{w_0}^{e_2}$ is upper bounded by $2/(W_0+1)$ and lower bounded by $2/(W_m+1)$. Putting everything together yields the result. $p_{c,i}^{e_2,\mathrm{CoS}}$ is derived using the same arguments. ■

Approximating $p_{w_0}^{e}$ by its upper bound is accurate when there are few collisions and data losses at the physical layer; otherwise, approximating it with its lower bound will be more accurate. Therefore, we make the following approximation:

$$p_{w_0}^{e} = \begin{cases} 2/(W_0+1), & \text{if } p_{l,0}^{e,\mathrm{CoS}} \le p_{\mathrm{cutoff}} \\ 2/(W_m+1), & \text{if } p_{l,0}^{e,\mathrm{CoS}} > p_{\mathrm{cutoff}} \end{cases}$$

where p_{cutoff} is the value of the DATA/ACK exchange loss probability that results in the lower and upper bound yielding the same error. (Its value for the default parameters of Table I is equal to 0.8.) This approximation is not introducing significant inaccuracies for the following reason. Assumption 2 implies that the probability of an RTS collision at some edge e due to another edge with which it forms a coordinated-stations topology is rather small (since the upper bound is small). On the other hand, the probability of RTS collisions due to edges with which e forms an asymmetric or far-hidden-edges topology (Sections III-B3 and III-B4) is much larger, and it dominates the calculation of the overall RTS collision probability. Finally, if there are only coordinated stations in e's neighborhood, the effect of the backoff counter being frozen due to carrier sensing will dominate over RTS collisions [see (1)]. Section V verifies that making this approximation has no significant impact on the accuracy of the analysis.

Finally, we derive the value of $p_{\mathrm{idle}}^{e_j,\mathrm{CoS}}$ in the next lemma. We use the following variable in this derivation. Let $K_{e,T}$ denote the expected number of DATA transmissions per packet at edge e in topology T, including the extra transmissions due to unsuccessful DATA–ACK exchange. Using elementary probability, $K_{e,T} = \sum_{i=1}^{m-1} i(1 - p_{l,i}^{e,T})(\prod_{k=1}^{i-1} p_{l,k}^{e,T}) + (\prod_{i=1}^{m-1} p_{l,i}^{e,T})(m - 1 + (1/(1 - p_{l,m}^{e,T})))$.

Lemma 3:

(i) $p_{\mathrm{idle}}^{e_1,\mathrm{CoS}} = (1 - K_{e_2,\mathrm{CoS}}\lambda_{e_2} T_s - \lambda_{e_1} T_s)/(1 - \lambda_{e_1} T_s)$;

(ii) $p_{\mathrm{idle}}^{e_2,\mathrm{CoS}} = (1 - K_{e_1,\mathrm{CoS}}\lambda_{e_1} T_s - \lambda_{e_2} T_s)/(1 - \lambda_{e_2} T_s)$.

Proof: The backoff counter for edge e_1 is frozen when a transmission at edge e_2 is going on, given that no successful transmission is going on at edge e_1.[4] The net rate at which packets are transmitted at edge e_2 is equal to $K_{e_2,\mathrm{CoS}}\lambda_{e_2}$, and T_s is the expected service time of one packet. Hence, the probability that there is a transmission ongoing at edge e_2 is equal to $K_{e_2,\mathrm{CoS}}\lambda_{e_2} T_s$. Notice that this derivation ignores the extra RTS–CTS traffic generated by an unsuccessful RTS–CTS exchange, but this is fully justified by the assumption that $T_{\mathrm{RTS}} \ll T_s$ (Assumption 1). Similarly, the probability that a successful packet transmission is going on at e_1 is equal to $\lambda_{e_1} T_s$. Putting everything together yields the result. $p_{\mathrm{idle}}^{e_2,\mathrm{CoS}}$ is derived using similar arguments. ■

Note that if there is no interference link between T_{e_1} and R_{e_2} in Fig. 2(a), then the probability of RTS collision at e_2 will be equal to 0 instead of $\lambda_{e_1} E[S_{e_1}] p_{w_0}^{e_1}$. Similarly, absence of the interference link between T_{e_2} and R_{e_1} will result in the probability of RTS collision at e_1 to be equal to 0.

2) Near Hidden Edges (NH): Fig. 2(b) shows the topology belonging to this category. T_{e_1} and T_{e_2} do not interfere with each other; however, there is an interference link between T_{e_1} and R_{e_2} as well as T_{e_2} and R_{e_1}. The values of $p_{l,i}^{e_j,\mathrm{NH}}$, $p_{c,i}^{e_j,\mathrm{NH}}$, and $p_{\mathrm{idle}}^{e_j,\mathrm{NH}}$, $0 \le i \le m$, $j = 1, 2$, are derived in a manner similar to the derivation of the corresponding probabilities for coordinated stations. The only difference is that now $T_{e_1}(T_{e_2})$ will freeze its backoff counter only when a CTS sent from $R_{e_2}(R_{e_1})$ is successfully received at $T_{e_1}(T_{e_2})$. So, the RTS transmitted by $T_{e_1}(T_{e_2})$ can now collide in the following four scenarios: 1) Both T_{e_1} and T_{e_2} start transmitting an RTS in the same slot

[4] If the RTS from T_{e_2} is successfully received at T_{e_1}, the backoff counter at T_{e_1} is frozen due to virtual carrier sensing, or else it is frozen due to physical carrier sensing. Hence, whenever there is a transmission on edge e_2, the backoff counter at e_1 is frozen.

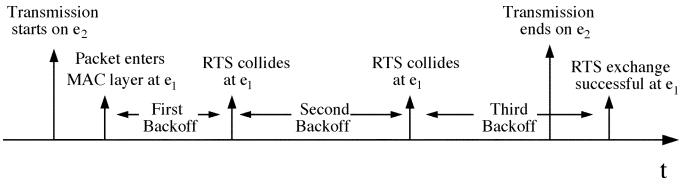

Fig. 3. Multiple RTS exchanges at e_1 can collide with the same DATA transmission on e_2 for the asymmetric topology.

duration; 2) $T_{e_1}(T_{e_2})$ starts transmitting an RTS, and $R_{e_2}(R_{e_1})$ starts transmitting a CTS in the same slot duration; 3) $T_{e_1}(T_{e_2})$ starts transmitting an RTS while $T_{e_2}(T_{e_1})$ is still sending an RTS; and 4) the CTS from $R_{e_2}(R_{e_1})$ is lost due to physical-layer errors at $T_{e_1}(T_{e_2})$.

3) Asymmetric Topology (AS): Fig. 2(c) shows an example of the topology belonging to this category. T_{e_1} and T_{e_2} as well as T_{e_1} and R_{e_2} do not interfere each other, but T_{e_2} and R_{e_1} are within each other's interference range. The main characteristic of this topology is that T_{e_2} is aware of the channel state as it can hear the CTS from R_{e_1}, but T_{e_1} is totally unaware of the channel state as it can hear neither the RTS nor the CTS from the transmission on e_2.

We first derive the collision and idle probabilities for edge e_1. The following lemma derives the value of $p_{l,i}^{e_1,\mathrm{AS}}$.

Lemma 4: $p_{l,i}^{e_1,\mathrm{AS}} = 1-(p_{\mathrm{DATA}}^{e_1} \times p_{\mathrm{ACK}}^{e_1}(1-p_{w_0}^{e_2}\lambda_{e_2}E[S_{e_2}])(1-P(E_{\mathrm{CTS}}^{R_{e_1},T_{e_2}})K_{e_2,\mathrm{AS}}\lambda_{e_2}T_s))$, $0 \le i \le m$. The expression for $K_{e,T}$ was derived in Section III-B1.

Proof: The DATA packet sent by T_{e_1} will collide if one of these two events happens: 1) If T_{e_2} starts transmitting an RTS and R_{e_1} starts transmitting a CTS in the same slot duration. 2) The CTS from R_{e_1} is not recovered at T_{e_2} due to physical-layer errors, and T_{e_2} starts a transmission as it is not aware of the ongoing transmission at e_1. ∎

We next derive the value of $p_{c,i}^{e_1,\mathrm{AS}}$ in the following sequence of lemmas. The first lemma directly follows from the observation that if T_{e_1} transmits an RTS while a transmission at edge e_2 is going on, it will collide. As before, note that this lemma ignores the extra RTS traffic generated at e_2 by an unsuccessful RTS–CTS exchange, which is not a problem since $T_{\mathrm{RTS}} \ll T_s$ (Assumption 1).

Lemma 5: $p_{c,0}^{e_1,\mathrm{AS}} = 1-(p_{\mathrm{RTS}}^{e_1} \times p_{\mathrm{CTS}}^{e_1}(1-K_{e_2,\mathrm{AS}}\lambda_{e_2}T_s))$. Now, lets look at what happens after the first RTS collision. The RTS collision will cause the backoff window at T_{e_1} to increase to W_1, and a new backoff counter is chosen uniformly at random between (0, W_1). If the remaining transmission time at edge e_2 is more than the new backoff counter, then the second RTS transmission at e_1 will collide with the same transmission. (Note that multiple RTS exchanges on e_1 can collide with the same DATA transmission on e_2, see Fig. 3.) Prior works have not incorporated this effect in their analysis, and hence, their accuracy decreases as T_s/W_0 increases. And if the remaining transmission time at edge e_2 is lower than the new backoff counter, then the probability of RTS collision is equal to $K_{e_2,\mathrm{AS}}\lambda_{e_2}T_s$. Therefore, $P(\mathrm{RTS/CTS}$ exchange is unsuccessful at the end of second backoff $|$ a collision occurred at the end of the first backoff$) = (1-p_0^1)+p_0^1 p_{c,0}^{e_1,\mathrm{AS}}$, where p_0^1 is the probability that the transmission at e_2, which collided with the first RTS transmission by T_{e_1} (when the backoff window at T_{e_1} was W_0), ends before the second backoff counter at T_{e_1} expires (when the backoff window at T_{e_1} is W_1). To evaluate $p_{c,1}^{e_1,\mathrm{AS}}$, note that the backoff window also increments if the first RTS–CTS exchange went through but the subsequent DATA or ACK packet was lost, in which case the RTS collision probability after the second backoff counter expires is equal to $K_{e_2,\mathrm{AS}}\lambda_{e_2}T_s$. Putting everything together yields $p_{c,1}^{e_1,\mathrm{AS}} = 1-(p_{\mathrm{RTS}}^{e_1} \times p_{\mathrm{CTS}}^{e_1}(1-((1-p_{\mathrm{RTS},0}^{e_1})p_{c,0}^{e_1,\mathrm{AS}}+p_{\mathrm{RTS},0}^{e_1}((1-p_0^1)+p_0^1 p_{c,0}^{e_1,\mathrm{AS}}))))$, where $p_{\mathrm{RTS},0}^{e_1,\mathrm{AS}} = K_{e_2,\mathrm{AS}}\lambda_{e_2}T_s/(p_{c,0}^{e_1,\mathrm{AS}}+(1-p_{c,0}^{e_1,\mathrm{AS}})p_{l,0}^{e_1,\mathrm{AS}})$ is the probability that an RTS collision occured at the end of the first backoff given that either the RTS/CTS exchange or the DATA/ACK exchange was unsuccessful at the end of the first backoff.

We now generalize the derivation of $p_{c,1}^{e_1,\mathrm{AS}}$ to find the value of $p_{c,i}^{e_1,\mathrm{AS}}, 1 \le i \le m$. We define the following variables for ease of presentation. a) Let $p_{\mathrm{RTS},i}^{e_1,\mathrm{AS}}$, $0 \le i \le m$, denote the probability that an RTS collision occurred at the end of the $(i+1)$th backoff given that either the RTS/CTS exchange or the DATA/ACK exchange was unsuccessful at the end of the $(i+1)$th backoff. If there is no RTS collision at the end of the $(i+1)$th backoff, then the probability of RTS/CTS exchange being unsuccessful at the end of the next backoff ($(i+2)$th backoff) is equal to $p_{c,0}^{e_1,\mathrm{AS}}$. b) Let $p_{\mathrm{RTS_{new}},i}^{e_1,\mathrm{AS}}$, $0 \le i \le m$, denote the probability that an RTS collision occurred at the end of the $(i+1)$th backoff given that i) either the RTS/CTS exchange or the DATA/ACK exchange was unsuccessful at the end of the $(i+1)$th backoff, and ii) the collision occurred with a transmission on e_2, which started when the backoff window at T_{e_1} was W_i, i.e., the colliding transmission on e_2 started while the backoff counter at T_{e_1} was decrementing during the $(i+1)$th backoff. This probability indicates the start of a new transmission at e_2, which might collide with the subsequent RTS exchanges. c) Let $E_{j,i}$ denote the event that an RTS collision occurred at e_1 when the backoff window at T_{e_1} was W_i, with a transmission on e_2 that had started when the backoff window at T_{e_1} was W_j. This event indicates the start of the ongoing transmission at e_2. d) Finally, let p_j^i denote the probability that a transmission at e_2, which started when the backoff window at T_{e_1} was W_j, ends when the backoff window at T_{e_1} is W_i given that it had not ended when the backoff window was W_{i-1}. This probability is used to count the number of RTS exchanges at e_1, which collides with the same transmission on e_2.

Lemma 6: $p_{c,i}^{e_1,\mathrm{AS}} = 1-(p_{\mathrm{RTS}}^{e_1} \times p_{\mathrm{CTS}}^{e_1}(1-(1-p_{\mathrm{RTS},i-1}^{e_1,\mathrm{AS}})p_{c,0}^{e_1,\mathrm{AS}}-\sum_{j=0}^{i-1}P(E_{j,i-1})(1-p_j^i+p_j^i p_{c,0}^{e_1,\mathrm{AS}})))$, $1 \le i \le m$.

Proof: Given event $E_{j,i-1}$ occurs, the probability that an RTS collision occurs when the backoff window at T_{e_1} is W_i is equal to $(1-p_j^i+p_j^i p_{c,0}^{e_1,\mathrm{AS}})$. On the other hand, if there is no RTS collision when the backoff window at T_{e_1} was W_{i-1}, the probability of RTS collision when the backoff window at T_{e_1} is W_i is equal to $p_{c,0}^{e_1,\mathrm{AS}}$. Combining everything together using the law of total probability yields the result. To complete the derivation of $p_{c,i}^{e_1,\mathrm{AS}}$, we have to derive the values of $P(E_{j,i})$, $p_{\mathrm{RTS},i}^{e_1,\mathrm{AS}}$, $p_{\mathrm{RTS_{new}},i}^{e_1,\mathrm{AS}}$, and p_j^i's. Values of these variables follow directly from their definitions. We omit their derivations due to space limitations. The interested reader is referred to [23]. ∎

The only remaining variable to be derived for edge e_1 is $p_{\mathrm{idle}}^{e_1,\mathrm{AS}}$. To derive its value, we use the fact that T_{e_1} cannot hear the transmission on e_2, and hence the channel at T_{e_1} is always idle.

Lemma 7: $p_{\text{idle}}^{e_1,\text{AS}} = 1$.

The next lemma states the value of the collision and idle probabilities for edge e_2. The proof directly follows from the following two observations: 1) No transmission from e_1 can collide at R_{e_2}, and 2) a CTS transmission from R_{e_1}, if successfully received by T_{e_2}, will freeze the backoff counter at T_{e_2} due to virtual carrier sensing.

Lemma 8:

(i) $p_{l,i}^{e_2,\text{AS}} = 1 - (p_{\text{DATA}}^{e_2} \times p_{\text{ACK}}^{e_2}), 0 \le i \le m$;

(ii) $p_{c,i}^{e_2,\text{AS}} = 1 - (p_{\text{RTS}}^{e_2} \times p_{\text{CTS}}^{e_2}), 0 \le i \le m$;

(iii) $p_{\text{idle}}^{e_2,\text{AS}} = (1 - (1 - P(E_{\text{CTS}}^{R_{e_1},T_{e_2}}))K_{e_1,\text{AS}}\lambda_{e_1}T_s - \lambda_{e_2}T_s)/(1 - \lambda_{e_2}T_s)$.

4) Far Hidden Edges (FH): Only R_{e_1} and R_{e_2} are within each other's range in this topology. Fig. 2(d) shows the topology belonging to this category. For this topology, an RTS sent by a transmitter will not receive a CTS back if a transmission is going on at the other edge because of virtual carrier sensing at the receiver. Thus, $p_{c,i}^{e_j,\text{FH}}$, $0 \le i \le m$, $j = 1,2$, is derived in a manner similar to the derivation of $p_{c,i}^{e_1,\text{AS}}$. The only difference occurs when the CTS from $R_{e_2}(R_{e_1})$ is lost at $R_{e_1}(R_{e_2})$, causing $R_{e_1}(R_{e_2})$ to be unaware of the channel state at $e_2(e_1)$ and sending a CTS back in response to the RTS from $T_{e_1}(T_{e_2})$. Hence, the probability of RTS collision is equal to the probability that there is a transmission ongoing at the other edge conditioned on the event that the CTS was correctly received. The probability of the event that the CTS is not correctly received is derived during the derivation of $p_{l,i}^{e_j,\text{FH}}$.

We next derive the value of the probability of DATA collisions. DATA on edge $e_1(e_2)$ will collide if $R_{e_2}(R_{e_1})$ transmits a CTS or an ACK. $R_{e_2}(R_{e_1})$ will send back a CTS only if it had not correctly received the CTS exchanged on $e_1(e_2)$. For this topology, DATA packets will not collide with ACK packets as the preceding RTS/CTS exchange on the other edge will cause the DATA to collide, and hence the receiver will not send back an ACK packet. We now have to determine the events that can cause $R_{e_2}(R_{e_1})$ to not correctly receive the CTS exchanged on $e_1(e_2)$.

Let us first consider edge e_1. Obviously, one of the events that can lead to the CTS getting corrupted is physical-layer errors. If either of the CTS from R_{e_2} to R_{e_1} or R_{e_1} to R_{e_2} gets corrupted, it will lead to DATA collision on edge e_1. Thus, the probability of DATA collision on edge e_1 due to the CTS getting corrupted by physical-layer errors is equal to $p_{l,\text{CTS}}^{e_1,\text{FH}} = (1 - (1 - P(E_{\text{CTS}}^{R_{e_1},R_{e_2}}))(1 - P(E_{\text{CTS}}^{R_{e_2},R_{e_1}})))K_{e_2,\text{FH}}\lambda_{e_2}T_s$.

We now describe events that can cause CTS to get corrupted due to collisions. Let $E_1^{e_1,\text{FH}}(E_2^{e_1,\text{FH}})$ denote the union of the following three events. 1) T_{e_1} and T_{e_2} start transmitting an RTS in the same slot duration with T_{e_1}'s (T_{e_2}'s) transmission starting first; 2) $T_{e_2}(T_{e_1})$ starts transmitting an RTS while an RTS transmission is going on at $e_1(e_2)$; and 3) $T_{e_2}(T_{e_1})$ starts transmitting an RTS in the same slot duration as $R_{e_1}(R_{e_2})$ starts transmitting a CTS. Neglecting T_{RTS} (easily justified by Assumption 1), $P(E_1^{e_1,\text{FH}}) = P(E_2^{e_1,\text{FH}}) = \lambda_{e_2}E[S_{e_2}]p_{w_0}^{e_2}$.

We now discuss the sequence of events which will follow event $E_1^{e_1,\text{FH}}(E_2^{e_1,\text{FH}})$. (Fig. 4 shows a possible realization of the sequence of events following event $E_1^{e_1,\text{FH}}$. Note that prior works have not incorporated the effect of the occurrence of events $E_1^{e_1,\text{FH}}$ and $E_2^{e_1,\text{FH}}$ in their analysis, and hence, their accuracy decreases as T_s/W_0 increases. a) The transmission

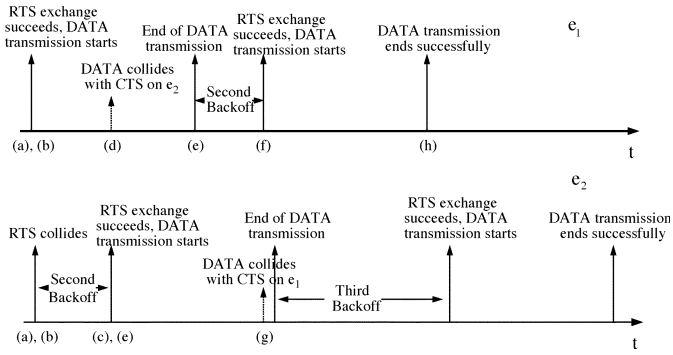

Fig. 4. A possible realization of the sequence of events that follow event $E_1^{e_1,\text{FH}}$.

of RTS on $e_1(e_2)$ will succeed, and $R_{e_1}(R_{e_2})$ will send back a CTS. This CTS will collide with the RTS transmission on $e_2(e_1)$ at $R_{e_2}(R_{e_1})$. This collision results in $R_{e_2}(R_{e_1})$ not receiving both the packets. b) DATA transmission will commence on $e_1(e_2)$, while $T_{e_2}(T_{e_1})$ backs off. c) Backoff counter at $T_{e_2}(T_{e_1})$ expires, and an RTS is transmitted on $e_2(e_1)$. $R_{e_2}(R_{e_1})$ responds back with a CTS. d) If the DATA transmission on $e_1(e_2)$ has not ended, the CTS transmission by $R_{e_2}(R_{e_1})$ in step c) will collide with the DATA transmission at $R_{e_1}(R_{e_2})$. e) $T_{e_1}(T_{e_2})$ backs off, and DATA transmission commences on $e_2(e_1)$. f) The backoff counter at $T_{e_1}(T_{e_2})$ expires and sends an RTS, and $R_{e_1}(R_{e_2})$ sends back a CTS. g) If the DATA transmission on $e_2(e_1)$ has not ended, the CTS transmission by $R_{e_1}(R_{e_2})$ will collide with the DATA transmission at $R_{e_2}(R_{e_1})$. h) This process goes on until at least one of the DATA packets get successfully exchanged.[5]

$p_{l,\text{CTS}}^{e_2,\text{FH}}$, $E_1^{e_2,\text{FH}}$, and $E_2^{e_2,\text{FH}}$ are similarly defined for edge e_2.

The value of $p_{l,i}^{e_j,\text{FH}}$, $0 \le i \le m$, is stated in the next lemma, whose proof follows directly from the discussion above. We define the following additional variables for ease of presentation. a) Let $p_{D,i}^{e_j,\text{FH}}$ denote the probability that a DATA collision occurs on e_j due to events $E_1^{e_j,\text{FH}}$ or $E_2^{e_j,\text{FH}}$ having occurred during previous exchanges, given the current backoff window at T_{e_j} is W_i and either the RTS/CTS or the DATA/ACK exchange was unsuccessful when the backoff window value at T_{e_j} was $W_0, \ldots W_{i-1}$. If the DATA/ACK loss does not occur due to events $E_1^{e_j,\text{FH}}$ or $E_2^{e_j,\text{FH}}$ having occurred during previous exchanges, the probability of DATA collision after the next backoff is equal to $p_{l,0}^{e_j,\text{FH}}$. b) Let $p_{D_{E_1},i}^{e_j,\text{FH}}(p_{D_{E_2},i}^{e_j,FH})$ denote the probability that event $E_1^{e_j,\text{FH}}(E_2^{e_j,\text{FH}})$ occurs during the current data exchange given that the current backoff window at T_{e_j} is W_i and either the RTS/CTS or the DATA/ACK exchange was unsuccessful when the backoff window value at T_{e_j} was

[5]Note that the loss of one of the RTS exchanges in this sequence due to physical-layer effects will change the probability of DATA collision. Ignoring this event is easily justifiable using Assumptions 1 and 2. By Assumption 1, the probability of the DATA packet getting corrupted by physical-layer errors will be much larger than the same probability for the RTS packet, as the DATA packets are much larger than the RTS packets. And $p_{l,i}^{e_1,\text{FH}}$, $0 \le i \le m$, will be dominated by $p_{\text{DATA}}^{e_1}$, as $P(E_1^{e_1,\text{FH}})$ and $P(E_2^{e_1,\text{FH}})$ are much smaller (by Assumption 2). Hence, for the network conditions for which $P(E_1^{e_1,\text{FH}})$ and $P(E_2^{e_1,\text{FH}})$ matter, ignoring the loss of RTS exchanges will introduce negligible error.

$W_0, \ldots W_{i-1}$. Event $E_1^{e_j,\mathrm{FH}}(E_2^{e_j,\mathrm{FH}})$ may be followed with a sequence of DATA collisions.

Lemma 9: For $j = 1, 2$, we have the following.

(i) $p_{l,0}^{e_j,\mathrm{FH}} = 1 - \Big[p_{\mathrm{DATA}}^{e_j} \times p_{\mathrm{ACK}}^{e_j}(1 - p_{l,\mathrm{CTS}}^{e_j,\mathrm{FH}}) \times (1 - P(E_1^{e_j,\mathrm{FH}}))\Big]$.

(ii) $p_{l,i}^{e_j,\mathrm{FH}} = 1 - \Big[p_{\mathrm{DATA}}^{e_j} \times p_{\mathrm{ACK}}^{e_j} \Big(1 - (1 - p_{D,i-1}^{e_j,\mathrm{FH}} - p_{D_{E_1},i-1}^{e_j,\mathrm{FH}} - p_{D_{E_2},i-1}^{e_j,\mathrm{FH}}) p_{l,0}^{e_j,\mathrm{FH}} - \sum_{k=0}^{i-1} p_{D_{E_1},k}^{e_j,\mathrm{FH}} \times \left(\frac{\prod_{u=k+1}^{i-1} p_{k,u}(E_1)}{\prod_{u=k+1}^{i-1} \times \left(p_{c,u}^{e_j,\mathrm{FH}} + (1 - p_{c,u}^{e_j,\mathrm{FH}}) p_{l,u}^{e_j,\mathrm{FH}}\right)} \right) \times \left(p_{k,i}(E_1) + p_{k,i}^{c}(E_1) p_{l,0}^{e_j,\mathrm{FH}}\right) - \sum_{k=0}^{i-1} p_{D_{E_2},k}^{e_j,\mathrm{FH}} \left(p_{k,i}(E_2) + p_{k,i}^{c}(E_2) p_{l,0}^{e_j,\mathrm{FH}}\right) \times \left(\frac{\prod_{u=k+1}^{i-1} p_{k,u}(E_2)}{\prod_{u=k+1}^{i-1} \left(p_{c,u}^{e_j,\mathrm{FH}} + (1 - p_{c,u}^{e_j,\mathrm{FH}}) p_{l,u}^{e_j,\mathrm{FH}}\right)} \right) \Big) \Big], \quad 1 \le i \le m.$

Derivation of the values of $p_{D,i}^{e_j,\mathrm{FH}}$, $p_{D_{E_l},i}^{e_j,\mathrm{FH}}$, $p_{j,i}(E_1)$, $p_{j,i}^{c}(E_1)$, $p_{j,i}(E_2)$, and $p_{j,i}^{c}(E_2)$ is omitted due to space limitations. The interested reader is referred to [23].

The only remaining variable to be derived is $p_{\mathrm{idle}}^{e_j,\mathrm{FH}}$. To derive its value, we use the fact that both transmitters cannot overhear each other.

Lemma 10: $p_{\mathrm{idle}}^{e_j,\mathrm{FH}} = 1, j = 1, 2$.

C. Determining the Achievable Edge-Rate Region in any Multihop Topology

To determine the edge-rate region for a given multihop topology T, recall that we first have to determine the expected service time at each edge, which in turn requires the values of $p_{c,i}^{e,T}$, $p_{l,i}^{e,T}$, and $p_{\mathrm{idle}}^{e,T}$ for each edge e. To derive these probabilities for an edge, we will decompose the local topology around the edge into a number of two-edge topologies, then find these probabilities for each two-edge topology, and finally find the net probability by appropriately combining the individual probabilities from each two-edge topology. We will use the flow-in-the-middle topology [Fig. 6(a)] as an example throughout the section.

Decomposition of the local topology around e is easily achieved by evaluating how each edge in e's neighborhood interferes with e, based on the definitions stated in Section III-B. For example, the local topology around edge $4 \rightarrow 5$ can be decomposed into the following two-edge topologies: 1) Coordinated stations: $5 \rightarrow 6$; 2) Near hidden edges: none; 3) Asymmetric topology: $2 \rightarrow 3$ and $8 \rightarrow 9$; and 4) Far hidden edges: $1 \rightarrow 2$ and $7 \rightarrow 8$. The previous section discussed how to find the collision and idle probabilities for each individual two-edge topology. This section focuses on how to combine the probabilities obtained from each individual two-edge topology.

Combining these probabilities must account for possible dependencies between the neighboring edges. For example, the transmitters of edges $1 \rightarrow 2$ and $2 \rightarrow 3$ in the flow-in-the-middle topology, which are both interfering with edge $4 \rightarrow 5$, can hear each other. Hence, DATA transmission on these two edges will not occur simultaneously. Thus, the collision probabilities due to these two edges cannot be combined independently to find the aggregate collision probabilities at $4 \rightarrow 5$.

We first present the scenarios where probabilities can be independently combined, and then discuss the scenarios where the dependencies have to carefully accounted for. The RTS and DATA collision probabilities can be independently combined if they are caused by two (or more) transmitters/receivers starting transmission in the same slot duration. For example, the RTS collision probability due to coordinated stations, and the DATA collision probability due to asymmetric topologies (if the CTS is received correctly at the other edge) can be independently combined. (For a complete list of events that can be independently combined, see the discussion following Lemmas 12 and 13.)

When the computation of any probability (either collision or idle probabilities) depends on the probability of the event that there is no ongoing transmission among a set of edges $\mathcal{N}$, dependencies have to be carefully accounted for and combining probabilities is more involved. For example, the computation of the RTS collision probability due to far-hidden-edges and asymmetric topologies and the computation of the DATA collision probability due to asymmetric topologies (if the CTS is not received correctly at the other edge) belong to this category. Also, the computation of the idle probability for coordinated-stations, near-hidden-edges, and asymmetric topologies belongs to this category. To understand how to compute the probability that there is no ongoing transmission among edges belonging to $\mathcal{N}$, it is helpful to distinguish between two types of dependencies that can exist between these edges.

Consider edge $4 \rightarrow 5$ in the flow-in-the-middle topology [Fig. 6(a)]. In this topology, edges $1 \rightarrow 2$ and $8 \rightarrow 9$ interfere with edge $4 \rightarrow 5$ but do not interfere with each other, whereas $1 \rightarrow 2$ and $2 \rightarrow 3$ interfere with both $4 \rightarrow 5$ and each other. Generalizing, 1) if two edges interfere with each other, then they will not be simultaneously scheduled (ignoring the extra RTS traffic due to the event that a colliding RTS transmission is taking place on both the edges, which is easily justified by Assumption 1), and 2) if two edges do not interfere with each other, then they can be independently scheduled, given that none of the edges that interfere with both are transmitting. For example, edges $2 \rightarrow 3$ and $8 \rightarrow 9$ will be independently scheduled, given there is no transmission ongoing at edges $4 \rightarrow 5$ and $5 \rightarrow 6$. Note that prior works do not incorporate the impact of these two dependencies [1) and 2)] in the evaluation of the collision and idle probabilities. We now state a lemma that finds the probability that there is an ongoing transmission on at least one of the edges in the given set $\mathcal{N}$. The lemma is derived using concepts from basic probability. In what follows, let X_e denote the event that there is a transmission going on at edge e, and note that $P(X_e) = K_{e,T}\lambda_e T_s$.

Lemma 11:

$$P\left(\cup_{e_n \in \mathcal{N}} X_{e_n}\right) = \sum_{e_i \in \mathcal{N}} P\left(X_{e_i}\right) - \sum_{e_i, e_j \in \mathcal{N}} P\left(X_{e_i} \cap X_{e_j}\right) + \ldots + (-1)^{|\mathcal{N}|-1} P\left(\cap_{e_i \in \mathcal{N}} X_{e_i}\right) \quad (2)$$

where for $\mathcal{N}_s \subseteq \mathcal{N}$, $P(\cap_{e_i \in \mathcal{N}_s} X_{e_i})$

$$= \begin{cases} 0, \text{ if any two edges in } \mathcal{N}_s \text{ interfere with each other} \\ \left(\prod_{e_i \in \mathcal{N}_s} P(X_{e_i})\right)/(1 - P(\cup_{e_k \in S_{\mathcal{N}_s}} X_{e_k}))^{|\mathcal{N}_s|-1}, \\ \quad \text{otherwise} \end{cases},$$

where $S_{\mathcal{N}_s}$ denotes the set of edges in E that interfere with all the edges in $\mathcal{N}_s$.

Based on the previous discussion, we can derive the collision and idle probability for each edge in a given multihop network. For completeness, we state the value of each probability in the

next three lemmas. The individual expressions are large because we combine the effect of each two-edge topology. However, each term in the expression can be traced to a term derived for one of the two-edge topologies.

We first define the notation used in these lemmas. Denote by $\mathcal{N}^e$ the set of edges that interfere with the edge under study e. Any edge $e_n \in E \setminus e$ that either forms a coordinated-stations or asymmetric topology or near hidden edge or far hidden edge with e belongs to this set. We subdivide the edges in $\mathcal{N}^e$ into subsets corresponding to the four two-edge topologies, and the coordinated station topologies and asymmetric topologies are further subdivided into two, giving us the following six sets: 1) $\mathcal{N}_1^e$: edges that form a coordinated station with e and interfere with the receiver of edge e; 2) $\mathcal{N}_2^e$: edges that form a coordinated station with e and do not interfere with the receiver of edge e; 3) $\mathcal{N}_3^e$: edges that form a near hidden edge with e; 4) $\mathcal{N}_4^e$: edges that form an asymmetric topology with e being the edge with an incomplete view of the channel state; 5) $\mathcal{N}_5^e$: edges that form an asymmetric topology with e being the edge that has the complete view of the channel state; and 6) $\mathcal{N}_6^e$: edges that form a far hidden edge with e. Edges in the sets $\mathcal{N}_1^e$, $\mathcal{N}_3^e$, $\mathcal{N}_4^e$, and $\mathcal{N}_6^e$ affect the RTS collision probabilities. Edges in the sets $\mathcal{N}_4^e$ and $\mathcal{N}_6^e$ affect the DATA collision probability. Edges in the sets $\mathcal{N}_1^e, \mathcal{N}_2^e, \mathcal{N}_3^e$. and $\mathcal{N}_5^e$ affect the proportion of idle time at the transmitter of e.

We first state the value of the DATA collision probability. We reuse the notations used in Lemmas 4 and 9. In a multihop topology, $P(E_1^{e,T}) = P(E_2^{e,T}) = 1-(\prod_{e_n\in\mathcal{N}_6^e}(1-\lambda_{e_n}E[S_{e_n}]p_{w0}^{e_n}))$. $p_{D,i}^{e,T}$, $p_{D_{E_1},i}^{e,T}$, and $p_{D_{E_2},i}^{e,T}$ are defined and derived similarly to the corresponding variables in Section III-B4. Also, based on the discussion in Section III-B1, we set

$$p_{w0}^{e_n} = \begin{cases} 2/(W_0+1), & \text{if } \mathcal{N}_4^{e_n}\cup\mathcal{N}_6^{e_n} = \phi \text{ and} \\ & p_{l,0}^{e_n,T} \le p_{\text{cutoff}} \\ 2/(W_m+1), & \text{otherwise.} \end{cases}$$

Lemma 12:

(i)

$$p_{l,0}^{e,T} = 1 - \Bigg(p_{\text{DATA}}^e \times p_{\text{ACK}}^e \times \Big[1 - P\Big(\big(\cup_{e_n\in\mathcal{N}_4^e} (X_{e_n} \cap E_{\text{CTS}}^{R_e,T_{e_n}}) \big) \cup \big(\cup_{e_n\in\mathcal{N}_6^e} (X_{e_n} \cap (E_{\text{CTS}}^{R_e,R_{e_n}} \cup E_{\text{CTS}}^{R_{e_n},R_e})) \big) \Big) \Big] \times \Bigg[\prod_{e_n\in\mathcal{N}_4^e} (1-\lambda_{e_n}E[S_{e_n}]p_{w0}^{e_n}) \Bigg] \big[1 - P(E_1^{e,T})\big] \Bigg).$$

(ii) $p_{l,i}^{e,T} = 1 - \Big(p_{\text{DATA}}^e \times p_{\text{ACK}}^e \Big(1 - \Big[(1 - p_{D,i-1}^{e,T} - p_{D_{E_1},i-1}^{e,T} - p_{D_{E_2},i-1}^{e,T}) p_{l,0}^{e,T} \Big] - \Big[\sum_{k=0}^{i-1} p_{D_{E_1},k}^{e,T} \times \Big(\frac{\prod_{u=k+1}^{i-1} p_{k,u}(E_1)}{\prod_{u=k+1}^{i-1} (p_{c,u}^{e,T} + (1-p_{c,u}^{e,T}) p_{l,u}^{e,T})} \Big) \times \big(p_{k,i}(E_1) + p_{k,i}^c(E_1) p_{l,0}^{e,T} \big) - \sum_{k=0}^{i-1} p_{D_{E_2},k}^{e,T} \times \big(p_{k,i}(E_2) + p_{k,i}^c(E_2) p_{l,0}^{e,T} \big) \times \Big(\frac{\prod_{u=k+1}^{i-1} p_{k,u}(E_2)}{\Big(\prod_{u=k+1}^{i-1} \big(p_{c,u}^{e,T} + (1-p_{c,u}^{e,T}) p_{l,u}^{e,T} \big) \Big)} \Big) \Big] \Big) \Big), 1 \le i \le m.$

In the expression of $p_{l,0}^{e,T}$, the first term within square brackets corresponds to the situation where a DATA collision is either caused by asymmetric topologies due to a CTS loss on the edge between the receiver of the edge under study, R_e, and the transmitter of a neighboring edge e_n, T_{e_n}, or far hidden edges due to CTS loss on the edge between R_e and R_{e_n}. The second term within square brackets corresponds to a DATA collision due to asymmetric topologies when T_e and R_{e_n} start transmitting a CTS the same time. The third term within square brackets denotes DATA collision following event $E_1^{e,T}$. In the expression of $p_{l,i}^{e,T}$, the two terms within square brackets correspond to the events where the previous exchange was not lost or lost due to DATA collisions following the events $E_1^{e,T}$ or $E_2^{e,T}$.

Derivation of the values of $p_{j,i}(E_1)$, $p_{j,i}^c(E_1)$, $p_{j,i}(E_2)$, and $p_{j,i}^c(E_2)$ is omitted due to space limitations. The interested reader is referred to [23]. Note that the events $X_{e_n}, \forall e_n \in E$ and the CTS getting lost on an edge are independent; hence, Lemma 11 is sufficient to derive $p_{l,i}^{e,T}$.

We next state the value of the RTS collision probability. We reuse the notation used in Lemma 6. Additionally, we define the event $X_{e,T} = (\cup_{e_n\in\mathcal{N}_3^e}(X_{e_n} \cap E_{\text{CTS}}^{R_{e_n},T_e})) \cup (\cup_{e_n\in\mathcal{N}_4^e} X_{e_n}) \cup (\cup_{e_n\in\mathcal{N}_6^e}(X_{e_n} \cap E_{\text{CTS}}^{R_{e_n},R_e}) \setminus (E_1^{e,T} \cup E_2^{e,T}))$, which denotes that there is at least one ongoing transmission that will cause an RTS collision at e.

Lemma 13:

(i) $p_{c,0}^{e,T} = 1 - (p_{\text{RTS}}^e \times p_{\text{CTS}}^e [\prod_{e_n\in\mathcal{N}_1^e}(1 - \lambda_{e_n}E[S_{e_n}]p_{w0}^{e_n})][\prod_{e_n\in\mathcal{N}_3^e}(1 - 2\lambda_{e_n}E[S_{e_n}]p_{w0}^{e_n})][1 - P(X_{e,T} \cup E_2^{e,T})])$,

(ii) $p_{c,i}^{e,T} = 1 - (p_{\text{RTS}}^e \times p_{\text{CTS}}^e (1 - [(1 - p_{\text{RTS},i-1}^{e,T}) p_{c,0}^{e,T}] - [\sum_{j=0}^{i-1} P(E_{j,i-1})(1 - p_j^i + p_j^i p_{c,0}^{e,T})]))$, $1 \le i \le m$.

In the expression for $p_{c,0}^{e,T}$, the first term within square brackets corresponds to RTS collisions due to coordinated stations, while the second term corresponds to RTS collisions due to near hidden edges when the CTS sent by R_{e_n} is successfully received at T_e. The third term corresponds to an RTS collision due to event $X_{e,T}$. In the expression for $p_{c,i}^{e,T}$, the two terms within square brackets correspond to the events where the previous exchange was not lost or lost due to the event $X_{e,T}$, respectively.

Please refer to [23] for the values of $P(E_{j,i})$, p_j^i, $p_{\text{RTS},i}^{e,T}$ and $p_{\text{RTS}_{\text{new}},i}^{e,T}$.

The next lemma states the value of $p_{\text{idle}}^{e,T}$. This lemma follows directly from the observation that any transmission on an edge belonging to $\mathcal{N}_1^e \cup \mathcal{N}_2^e$ will freeze the backoff counter on e, and any transmission on an edge belonging to $\mathcal{N}_3^e \cup \mathcal{N}_5^e$ will freeze the backoff counter on e only if the corresponding CTS is correctly received at T_e.

Lemma 14: $p_{\text{idle}}^{e,T} = (1 - P((\cup_{e_n\in\mathcal{N}_1^e\cup\mathcal{N}_2^e} X_{e_n}) \cup (\cup_{e_n\in\mathcal{N}_3^e\cup\mathcal{N}_5^e}(X_{e_n} \cap \bar{E}_{\text{CTS}}^{R_{e_n},T_e}))) - \lambda_e T_s)/(1 - \lambda_e T_s)$, where $\bar{E}_{\text{CTS}}^{R_{e_n},T_e}$ denotes the complement of event $E_{\text{CTS}}^{R_{e_n},T_e}$.

Equation (1) and the expressions derived in this section enable the derivation of the expected service time at any edge in any multihop topology. Thus, these equations along with the constraints $\sum_{e\in O_v} \lambda_e E[S_e] < 1, \forall v \in V$, (where O_v represents the set of outgoing edges from a node v) characterize the achievable rate region Λ_E. We sum over all outgoing edges from a node because the network queue for all outgoing edges at a

node is the same. (Note that, unlike prior works, the proposed methodology can be applied to topologies with nodes having multiple outgoing edges.)

Finally, we now comment on the computational complexity of setting up the equations for each edge. The complexity of the algorithm to decompose the local topology around an edge e into its constituent two-edge topologies is polynomial in $|\mathcal{N}^e|$. Computing the collision and idle probability for each two-edge topology takes constant time. Finally, the complexity of the algorithm to combine the individual collision and idle probabilities is equal to the number of nonzero terms in (3). Each nonzero term in this equation corresponds to a distinct set of noninterfering edges in $\mathcal{N}^e$. Therefore, the number of nonzero terms taking an intersection over $1 \leq j \leq |\mathcal{N}^e|$ edges is equal to the number of distinct sets of j noninterfering edges, which is $O(|\mathcal{N}^e|^j)$. However, the maximum number of noninterfering edges in $\mathcal{N}^e$ is bounded by a constant in practical topologies [24]. Hence, the number of nonzero terms in (3) is polynomial in $|\mathcal{N}^e|$. Therefore, the overall computational complexity of setting up equations for an edge e is polynomial in $|\mathcal{N}^e|$.

D. Network Solution

Determining the expected service time of all edges requires solving a coupled multivariate system of equations. We adopt an iterative procedure that uses the values of the idle and collision probabilities computed in the previous iteration for the current iteration. Proving the existence and uniqueness of a fixed point and convergence of this iterative procedure to this fixed point is out of scope and left as future work. The interested reader is referred to [25] and [26] for related fixed-point theory.

We now give some insight into the complexity associated with these proofs. The same iterative procedure has been used to solve the multivariate equations arising in both 802.11-scheduled single-hop [21], [27] and multihop networks [15], [17]. Note that single-hop networks are *topologically* homogeneous, and hence the same fixed-point equation governs the collision probability at each node. In contrast, for multihop networks, the fixed-point equation governing the collision and idle probabilities are different for each node; even the structure of these equations can differ for each node. Hence, proving uniqueness and convergence results is significantly more involved for multihop networks. Even for the simpler setting of single-hop networks, only a recent work [28] has derived conditions for the uniqueness of a fixed-point solution for the most general cases where nodes can be parametrically heterogeneous (but topologically homogeneous). Meanwhile, convergence of the iterative procedure is still not well understood. No progress has been made in the context of multihop networks yet.

In the absence of formal proofs, prior works have relied on extensive simulations to assess the convergence of the iterative procedure. We have adopted the same approach and performed extensive simulations on almost 30 representative topologies. For these topologies, the average number of iterations to converge was 6 and the maximum was 8, irrespective of the initial conditions. For a detailed description of these topologies, please see Section V.

IV. Achievable Flow-Rate Region

The achievable flow-rate region of a given multihop network and a collection of source–destination pairs is characterized by the set of the following constraints:

$$
\begin{aligned}
r_f &\geq 0 \quad \forall f \in \mathcal{F} \\
\lambda_e &= \sum_{f \in \mathcal{F}} r_f^e \quad \forall e \in E \\
g(f) + \sum_{e \in I_v} r_f^e &= \sum_{e \in O_v} r_f^e \quad \forall f \in \mathcal{F}, \forall v \in V \\
\vec{\lambda}_e &\in \Lambda_E
\end{aligned}
$$

where r_f^e denotes the flow rate of flow f flowing through edge e

$$
g(f) = \begin{cases} r_f, & \text{if } v = s(f) \\ -r_f, & \text{if } v = d(f) \\ 0, & \text{otherwise} \end{cases}
$$

and I_v and O_v denote the set of incoming edges into and outgoing edges from the node v, respectively. The first constraint ensures nonnegativity of flow rates, the second expresses edge rates in terms of flow rates, and the third is the standard flow conservation constraint. The final constraint says that the vector of edge rates $\vec{\lambda}_e$ induced at the edges should lie within the achievable edge-rate region.

V. Model Verification

In this section, we verify the accuracy of the analysis by finding the achievable-rate region for the four two-edge topologies and five different multihop topologies via simulations and comparing it to the theoretically derived achievable rate region. The multihop topologies we use are either characteristic representative topologies, real topologies, or randomly generated topologies. We also include the achievable rate region of optimal scheduling, derived using the methodology proposed by Jain *et al.* [1], to shed light on how far from the optimal 802.11 is. Furthermore, motivated by prior work that has expressed concerns about the ability to achieve fair and efficient rate allocations under 802.11 [11], [15], [29], we compare the max-min rate allocation under 802.11 and under an optimal scheduler.

To ensure that the difference between 802.11 and optimal scheduling is only due to the scheduling inefficiencies of 802.11, we make the overhead imposed by control message exchange and protocol headers to be the same for both schemes. (In practice, the overhead of optimal scheduling is expected to be larger, but this is besides the point here.)

A. Two-Edge Topologies

We plot the achievable edge-rate regions derived analytically and via simulations for the four two-edge topologies in Fig. 5(a)–(d). We make the following observations from these figures. 1) A close match between the analytical and simulation results verifies the accuracy of the analysis. 2) The asymmetric topology has the smallest achievable-rate region among the four two-edge topologies, which implies that the loss in throughput with 802.11 scheduling is largest for this topology. On the other hand, the coordinated station topology has the largest achievable-rate region. 3) In the asymmetric topology, even though 802.11 is highly unfair to e_1 in saturation conditions (see arrow in the figure) as also observed in [15], with rate control, it is possible to achieve a max-min rate allocation of 0.277 Mbps/edge, which is not that far from the max-min rate allocation of 0.332 Mbps/edge achieved by an optimal scheduler.

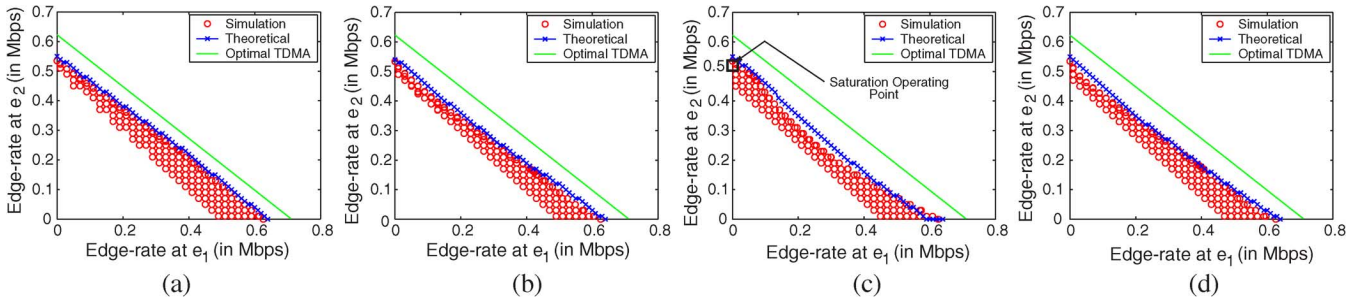

Fig. 5. Capacity regions for different two-edge topologies. The packet-loss rate for a 1024-byte packet is equal to 0.2 at e_1, 0.3 at e_2, and 0.5 at all the interference links. (All the rates are in Mbps.) (a) Coordinated stations. (b) Near hidden edges. (c) Asymmetric topology. (d) Far hidden edges. (The error in the maximum rate achieved at e_1 after fixing the rate at e_2 is less than 10.1% for all four plots.)

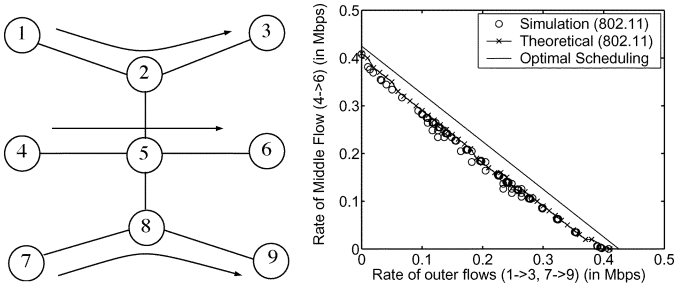

Fig. 6. (a) The flow-in-the-middle topology. (b) Achievable-rate region for the flow-in-the-middle topology.

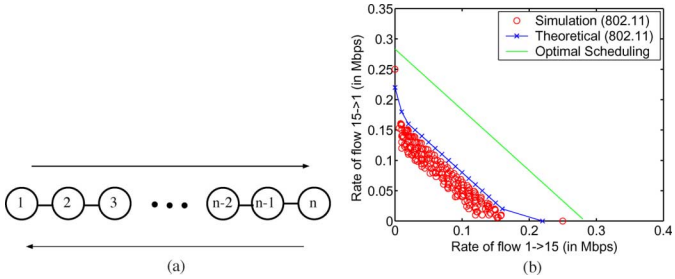

Fig. 7. (a) Chain topology. (b) Achievable-rate region for the chain topology.

B. Common Topologies

The first two multihop topologies we consider have been used by prior works to study the performance of 802.11 in multihop networks: a) Flow-in-the-middle topology, which was used in [8], [11], and [30]; and b) Chain topology, which was used in [7], [29], and [31].

1) Flow-in-the-Middle Topology: Fig. 6(a) shows the flow-in-the-middle topology. All links are assumed to be lossless. There are three flows in this topology: $1 \rightarrow 3$, $4 \rightarrow 6$, and $7 \rightarrow 9$. Flows $1 \rightarrow 3$ and $7 \rightarrow 9$ do not interfere with each other, but both of them interfere with flow $4 \rightarrow 6$.[6]

Since flows $1 \rightarrow 3$ and $7 \rightarrow 9$ are symmetric, we assume that they have equal rates. We plot the achievable rate of these two flows against the achievable rate for the middle flow $(4 \rightarrow 6)$ in Fig. 6(b). We make the following observations from this figure. 1) The analytical and simulation curves are close to each other, verifying the accuracy of the analysis. We compare the error between simulations and analysis for the maximum rate achieved by flow $4 \rightarrow 6$ when the rates of flows $1 \rightarrow 3$ and $7 \rightarrow 9$ are fixed. The error is less than 9%. Note that comparing the achievable flow-rate region also verifies the analysis presented in Section III, as the induced edge rates should lie within the achievable edge-rate region for a set of flow rates to be achievable (see Section IV). 2) The achievable-rate region with 802.11 scheduling is not convex. 3) The max-min rate allocation for this topology with 802.11 is 0.194 Mbps/flow and is 0.213 Mbps/flow with optimal scheduling. Thus, 802.11 achieves 91% throughput compared to optimal scheduling at the max-min rate allocation.

2) Chain Topology: Fig. 7(a) shows the chain topology. All links are assumed to be lossless. We set $n = 15$. There are two flows in this topology: $1 \rightarrow 15$ and $15 \rightarrow 1$. We plot the achievable-rate region of these two flows in Fig. 7(b). We make the following observations from this figure. 1) The analytical and simulation curves are close to each other, verifying the accuracy of the analysis. We compare the error between simulations and analysis for the maximum rate achieved by flow $1 \rightarrow 15$ when the rate of flow $15 \rightarrow 1$ is fixed. The error is less than 12%. 2) The achievable-rate region with 802.11 scheduling is not convex for this topology as well. 3) The max-min rate allocation for this topology with 802.11 is 0.09 Mbps/flow and is 0.14 Mbps/flow with optimal scheduling. Thus, 802.11 achieves 64.3% throughput compared to optimal scheduling at the max-min rate allocation.

C. Square Topology: Which Route

The next topology we study is the square topology of Fig. 8(a). All links are assumed to be lossless. There are two flows present in this topology: $1 \rightarrow 8$ and $8 \rightarrow 1$. There are two possible routes for each flow: $1 \rightarrow 2 \rightarrow 3 \rightarrow 4 \rightarrow 8$ and $1 \rightarrow 5 \rightarrow 6 \rightarrow 7 \rightarrow 8$ for flow $1 \rightarrow 8$, and $8 \rightarrow 4 \rightarrow 3 \rightarrow 2 \rightarrow 1$ and $8 \rightarrow 7 \rightarrow 6 \rightarrow 5 \rightarrow 1$ for flow $8 \rightarrow 1$. We use his topology to illustrate that our analysis yields the optimal routes as a by-product and show that 802.11 and optimal scheduling can have different optimal routes.

We plot the achievable-rate region for this topology in Fig. 8(b). We make the following observations from this figure. 1) Again, the simulation and analytical curves are close to each other. The error in the maximum rate achieved by flow $8 \rightarrow 1$ when the rate of flow $1 \rightarrow 8$, if fixed, is less than 14%. 2) The maximum throughput with 802.11 when only one of the flows is on is equal to 0.33 Mbps (point A in the figure) and is achieved by routing 0.165 Mbps along one path and 0.165 Mbps along the other. 3) When both flows are on, the max-min point with 802.11 (point B in the figure) is achieved by single-path routing with nonoverlapping routes for the two

[6]We say that two flows interfere with each other if any two edges over which they are routed interfere with each other.

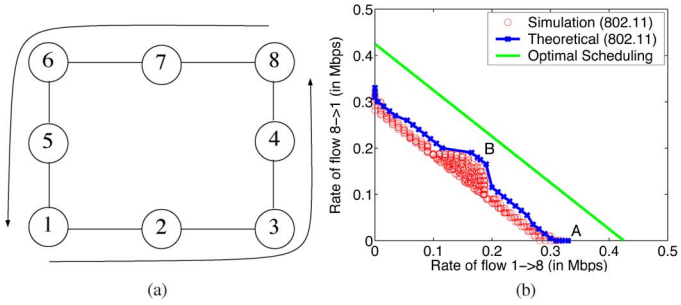

Fig. 8. (a) Square topology. (b) Achievable-rate region for the square topology.

flows, for example $1 \rightarrow 8$ routed along $1 \rightarrow 2 \rightarrow 3 \rightarrow 4 \rightarrow 8$ and flow $8 \rightarrow 1$ routed along $8 \rightarrow 7 \rightarrow 6 \rightarrow 5 \rightarrow 1$. However, optimal scheduling can achieve the max-min point by both single-path and multipath routing. Thus, the optimal routing paths for 802.11 and optimal scheduling can be different. 4) The max-min rate allocation with 802.11 is 0.18 Mbps/flow and is 0.213 Mbps/flow with optimal scheduling. Thus, 802.11 achieves 84.5% throughput compared to optimal scheduling at the max-min rate allocation.

D. A Real Topology: Houston Neighborhood

The next topology we choose is the real topology of an outdoor residential deployment in a Houston neighborhood [6]. The node locations (shown in Fig. 9) are derived from the deployment and fed into the simulator. The physical channel that we use in the simulator is a two-ray path loss model with Log-normal shadowing and Rayleigh fading [32]. The ETX routing metric [33] (based on data loss in absence of collisions) is used to set up the routes. Nodes 0 and 1 are connected to the wired world and serve as gateways for this deployment. All other nodes route their packets toward one of these nodes (whichever is closer in terms of the ETX metric). The resulting topology as well as the routing tree is also shown in Fig. 9. The loss rates at each link are determined from the simulator by letting each node send several broadcast messages one by one and measure the number of packets successfully received at every other node. The topology information and loss rates are fed into the analytical model to find the achievable-rate region for this topology. There are 16 flows in this topology. Hence, we only compare the max-min rate allocation from simulations and theory. A very good match is observed: The simulator allocates 46 Kbps/flow, whereas the theory allocates 44 Kbps/flow $(\text{error} = 4.4\%)$. Optimal scheduling allocates 67.3 Kbps/flow at the max-min rate allocation. Thus, 802.11 achieves 65.3% of the throughput compared to optimal scheduling at the max-min rate allocation.

E. Random Topology

We create the final topology by randomly placing 75 nodes in a 1000 m $\times$ 1000 m area. Both transmission and interference range are set equal to 200 m. We assume links used for routing packets to be lossless and assume $p^e_{\text{RTS}} = p^e_{\text{CTS}} = 0.4$ on all the other links since links used in routing paths typically are low-loss links. We select six source–destination pairs at random. We compare the max-min rate allocation from simulations and theory. A very good match is observed: The simulator allocates 94 Kbps to five of the flows and 650 Kbps to the sixth

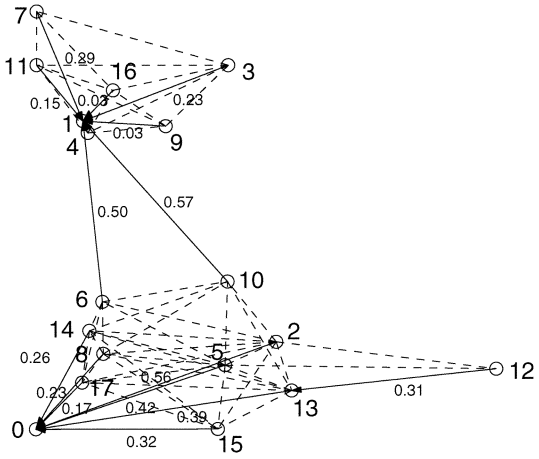

Fig. 9. Topology from the deployment in a Houston neighborhood. Arrows show the routing paths and the numerals on top of an arrow is the probability of loss of a 1024 byte packet on that link. Dashed lines represent the interference links.

flow, whereas theory allocates 96 Kbps to five of the flows and 600 Kbps to the sixth flow $(\text{error} = 7.6\%)$. Optimal scheduling allocates 141.7 Kbps to five of the flows and 706 Kbps to the sixth flow at the max-min rate allocation. Thus, at the max-min point, 802.11 achieves 76.35% of the total sum throughput compared to optimal scheduling.

F. Different Network Parameters

All the previous comparisons were made for a particular set of network parameters. In this section, we investigate the accuracy of the analysis when the network parameters are modified from their default values. We compare the achievable-rate region derived via simulations and theory for the flow-in-the-middle topology [Fig. 6(a)] for: 1) 100-byte DATA packets at 1-Mbps data rate in Fig. 10(a); and 2) 1024-byte packets at 11-Mbps data rate in Fig. 10(b). The error between simulations and analysis for the maximum rate achieved by flow $4 \rightarrow 6$ when the rates of flows $1 \rightarrow 3$ and $7 \rightarrow 9$ are fixed is less than 15% for both scenarios. Note that for both the scenarios, Assumption 1 does not hold, and hence we see a larger error. For smaller DATA packets, the reason why Assumption 1 does not hold is obvious. However, why increasing the data rate to 11 Mbps makes this assumption invalid is not obvious as the DATA packet size is still two orders of magnitude larger than the RTS packet size. In 802.11, the PHY header contains information used to determine the data rate of the incoming transmission (to allow auto-rate adaptation [20]), and hence is always transmitted at 1 Mbps. And the PHY layer header is exchanged for both control and DATA packets. Hence, the transmission time of a RTS packet becomes comparable to the transmission time of a DATA packet, which violates Assumption 1. Note that this is a protocol issue that needs to be fixed since this violates the basic protocol design premise that the load due to control packets should be a small fraction of the total load.

From Fig. 10(a) and (b), we also observe that 802.11 achieves more than 84% throughput at the max-min rate allocation compared to optimal scheduling for both the scenarios. Note that, in both these examples, the overhead is significantly larger than in previous scenarios.

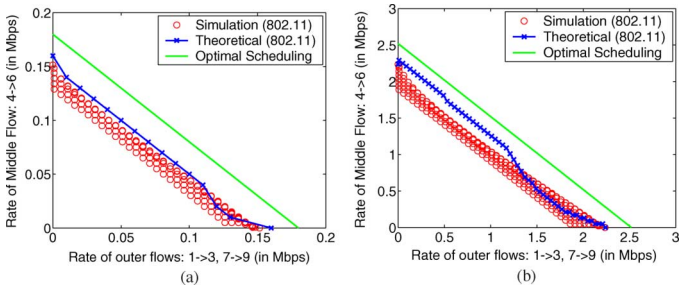

Fig. 10. (a) Achievable-rate region for the flow-in-the-middle topology for 100-byte packets and 1-Mbps data rate. (b) Achievable-rate region for the flow-in-the-middle topology for 1024-byte packets and 11-Mbps data rate.

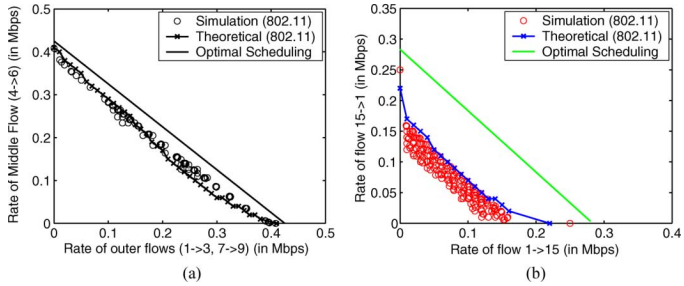

Fig. 11. (a) Achievable-rate region for the flow-in-the-middle topology with the approximations of Section VI. Error between simulations and analysis is less than 20%. (b) Achievable-rate region for the chain topology with the approximations of Section VI. Error between simulations and analysis is less than 12%.

G. Summary

We now summarize the observations made in this section. 1) Under the assumptions we make, our analysis is accurate as we incorporate all the events leading to collisions/busy channel in our proofs. Our assumptions are shown to be accurate via simulations since the analytical results have an average error of 9% and a maximum error of 15%. 2) The achievable-rate region with 802.11 scheduling is nonconvex. 3) 802.11 achieves more than 64% throughput compared to optimal scheduling at the max-min rate allocation for all the topologies studied in this paper. This is an interesting and unexpected observation. A prior work of ours [34] attempts to understand the optimality of 802.11. However, characterizing the worst-case performance of 802.11 is still an open question and left for future work. 4) The optimal routing paths for 802.11 and optimal scheduling can be different.

Note that the above summary results are based on simulation studies over almost 30 representative topologies. (Limitations of space allowed us to only show results for nine of them in the paper.) These include a number of characteristic topologies, including the flow-in-the-middle topology (Section V-B1) and variations, chain-like topologies (like the one in Section V-B2), tree-like topologies, star-like topologies, ring-like topologies, and the square topology in Section V-C. They also include a number of random topologies (see Section V-E for one of them), and the real Houston neighborhood topology presented in Section V-D.

VI. Network Solution Without the Iterative Procedure

As discussed in Section III-D, we need an iterative procedure to solve the coupled multivariate system of equations derived in Section III. In this section, we discuss if it is possible to decouple the equations to avoid using an iterative procedure by sacrificing some accuracy in the analysis. We look at the following questions. 1) Under what network conditions can the equations be decoupled without an unreasonable loss in accuracy? 2) What are the approximations to be made to remove the coupling?

A careful look at Lemmas 11 and 12 and the expression for $K_{e,T}$ derived in Section III-B1 tells us that the equations cannot be decoupled for networks with a nonnegligible probability of RTS/CTS loss on edges without a significant loss in accuracy.

For networks with a negligible probability of RTS/CTS loss, one can make the following two approximations to decouple the equations. The first approximation is to replace $\lambda_e E[S_e]$ by $\min(\lambda_e/\lambda_{\text{sat},n_e}, 1)$ in the expressions for the following two probabilities: 1) the DATA collision probability (Lemma 12), and 2) the RTS collision probability (Lemma 13). $\lambda_{\text{sat},n}$ denotes the saturation throughput of a WLAN with n transmitters transmitting to a single receiver (derived in [21]), and $n_e = |\mathcal{N}_e|$ is the number of edges interfering with e. Note that $\lambda_e E[S_e]$ is upper-bounded by 1. Since approximating $\lambda_e E[S_e]$ by its upper bound is inaccurate when λ_e is small, in these situations we replace $E[S_e]$ by $1/\lambda_{\text{sat},n_e}$. ($\lambda_{\text{sat},n}$ as a function of n flattens out rather fast [21]. As a result, even if just a few neighboring edges are saturated, $1/\lambda_{\text{sat},n}$ would be a good lower bound since the topology that minimizes service times is the one where all nodes are within range.) The second approximation is to approximate $P(\cap_{e_i \in \mathcal{N}_s} X_{e_i}) = (\prod_{e_i \in \mathcal{N}_s} P(X_{e_i}))/(1 - P(\cup_{e_k \in S_{\mathcal{N}_s}} X_{e_k}))^{|\mathcal{N}_s|-1}$ when no two edges in $\mathcal{N}_s$ interfere with each other in Lemma 11 with $(\prod_{e_i \in \mathcal{N}_s} P(X_{e_i}))/(1 - \sum_{e_k \in S_{\mathcal{N}_s}} P(X_{e_k}))^{|\mathcal{N}_s|-1}$.

With the first approximation, the DATA collision probabilities can be derived for each edge independently. Now, given the DATA collision probabilities at each edge, with the second approximation, one can find the RTS collision probabilities and idle probability at each edge independently.

Using these approximations will introduce some inaccuracies. However, for the topologies studied in this paper, the inaccuracies are not large. For example, Fig. 11(a) and (b) compare the achievable-rate region derived with these approximations to the simulation results for the flow-in-the-middle topology and the chain topology, respectively. With the two approximations, the maximum error is less than 20% for both the topologies.

VII. Conclusion and Future Work

In this paper. we have characterized the capacity region of an arbitrary multihop wireless network with 802.11 scheduling by deriving a methodology to characterize the achievable edge-rate region. This paper is a precursor to several works that require a general and accurate characterization of the achievable-rate region of 802.11-scheduled multihop networks. We briefly describe three such ongoing works.

Optimality of 802.11: In Section V, we observed that 802.11 achieves more than 64% throughput compared to optimal scheduling at the max-min rate allocation for all the topologies we studied. These results serve as a motivation to understand the worst-case performance of 802.11.

Optimal Routing and Rate Allocation: The constraints characterizing the achievable flow-rate region of a given 802.11-scheduled multihop network (Section IV) can be fed into an optimization problem to find optimal routing and rate allocation for different utility functions.

Residual Bandwidth Estimation: The methodology of Section III can be used to find the residual bandwidth at a given edge, given the edge rates at the other edges in the network. This can be used to design interference-aware routing [16], [36] or a congestion control algorithm that sends explicit and precise rate feedback to the sources (for example, see our recent work [37]).

REFERENCES

[1] K. Jain, J. Padhye, V. Padmanabhan, and L. Qiu, "Impact of interference on multi-hop wireless network performance," in *Proc. ACM MOBICOM*, 2003, pp. 66–80.

[2] V. Kumar, M. Marathe, S. Parthasarathy, and A. Srinivasan, "Algorithmic aspects of capacity in wireless networks," in *Proc. ACM Sigmetrics*, 2005, pp. 133–144.

[3] J. Bicket, D. Aguayo, S. Biswas, and R. Morris, "Architecture and evaluation of an unplanned 802.11b mesh network," in *Proc. ACM MOBICOM*, 2005, pp. 31–42.

[4] D. Raychaudhuri, I. Seskar, M. Ott, S. Ganu, K. Ramachandran, H. Kremo, R. Siracusa, H. Liu, and M. Singh, "Overview of the orbit radio grid testbed for evaluation of next-generation wireless network protocols," in *Proc. IEEE WCNC*, 2005, vol. 3, pp. 1664–1669.

[5] J. Eriksson, S. Agarwal, P. Bahl, and J. Padhye, "Feasibility study of mesh networks for all-wireless offices," in *Proc. ACM MOBISYS*, 2006, pp. 69–82.

[6] J. Camp, J. Robinson, C. Steger, and E. Knightly, "Measurement driven deployment of a two-tier urban mesh access network," in *Proc. ACM MOBISYS*, 2006, pp. 96–109.

[7] S. Ray, D. Starobinski, and J. Carruthers, "Performance of wireless networks with hidden nodes: A queuing-theoretic analysis," *J. Comput. Commun.*, vol. 28, pp. 1179–1192, 2005.

[8] C. Chaudet, I. Lassous, and B. Gaujal, "Study of the impact of asymmetry and carrier sense mechanism in IEEE 802.11 multi-hops networks through a basic case," in *Proc. PE-WASUN'04*, 2004, pp. 1–7.

[9] H. Chaya and S. Gupta, "Performance modeling of asynchronous data transfer methods of IEEE 802.11 mac protocol," *ACM Wireless Netw.*, vol. 3, pp. 217–234, 1997.

[10] M. Carvalho and J. Garcia-Luna-Aceves, "A scalable model for channel access protocols in multihop ad-hoc networks," in *Proc. ACM MOBICOM*, 2004, pp. 330–344.

[11] X. Wang and K. Kar, "Throughput modeling and fairness issues in CSMA/CA based ad-hoc networks," in *Proc. IEEE INFOCOM*, 2005, pp. 23–34.

[12] C. Reis, R. Mahajan, M. Rodrig, D. Wetherall, and J. Zahorjan, "Measurement-based models of delivery and interference," in *Proc. ACM SIGCOMM*, 2006, pp. 51–62.

[13] H. Chang, V. Misra, and D. Rubenstein, "A general model and analysis of physical layer capture in 802.11 networks," in *Proc. IEEE INFOCOM*, 2006.

[14] A. Kashyap, S. Ganguly, and S. Das, "A measurement-based approach to modeling link capacity in 802.11-based wireless networks," in *Proc. ACM MOBICOM*, 2007, pp. 242–253.

[15] M. Garetto, T. Salonidis, and E. Knightly, "Modeling per-flow throughput and capturing starvation in CSMA multi-hop wireless networks," in *Proc. IEEE INFOCOM*, 2006.

[16] Y. Gao, D. Chiu, and J. Lui, "Determining the end-to-end throughput capacity in multi-hop networks: Methodology and applications," in *Proc. ACM Sigmetrics*, 2006, pp. 39–50.

[17] K. Medepalli and F. A. Tobagi, "Towards performance modeling of IEEE 802.11 based wireless networks: A unified framework and its applications," in *Proc. IEEE INFOCOM*, 2006.

[18] L. Qiu, Y. Zhang, F. Wang, M. Han, and R. Mahajan, "A general model of wireless interference," in *Proc. ACM MOBICOM*, 2007, pp. 171–182.

[19] S. M. Das, D. Koutsonikolas, Y. C. Hu, and D. Peroulis, "Characterizing multi-way interference in wireless mesh networks," in *Proc. ACM WinTECH Workshop*, 2006, pp. 57–64.

[20] *Part 11: Wireless LAN Medium Access Control (MAC) and Physical Layer (PHY) Specifications—Higher-Speed Physical Layer Extension in the 2.4 GHz Band*, IEEE Std 802.11b-1999, Nov. 2002.

[21] G. Bianchi, "Performance analysis of the IEEE 802.11 distributed coordination function," *IEEE J. Sel. Areas Commun.*, vol. 18, no. 3, pp. 535–547, Mar. 2000.

[22] G. Sharma, A. Ganesh, and P. Key, "Performance analysis of contention based medium access control protocols," in *Proc. IEEE INFOCOM*, 2006.

[23] A. Jindal and K. Psounis, "Characterizing the achievable rate region of wireless multi-hop networks with 802.11 scheduling," Univ. of Southern California, Tech. Rep. CENG-2007-12, 2007.

[24] P. Chaporkar, K. Kar, X. Luo, and S. Sarkar, "Throughput and fairness guarantees through maximal scheduling in wireless networks," *IEEE Trans. Inf. Theory*, vol. 54, no. 2, pp. 572–594, Feb. 2008.

[25] V. I. Istratescu, *Fixed Point Theory, An Introduction*. Dordrecht, The Netherlands: D. Reidel, 1981.

[26] A. Granas and J. Dugundji, *Fixed Point Theory*. New York: Springer-Verlag, 2003.

[27] D. Malone, K. Duffy, and D. Leith, "Modeling the 802.11 distributed coordination function in nonsaturated heterogeneous conditions," *IEEE/ACM Trans. Netw.*, vol. 15, no. 1, pp. 159–172, Feb. 2007.

[28] V. Ramaiyan, A. Kumar, and E. Altman, "Fixed point analysis of single cell IEEE 802.11e WLANs: Uniqueness, multistability and throughput differentiation," in *Proc. ACM Sigmetrics*, 2005, pp. 109–120.

[29] M. Durvy, O. Dousse, and P. Thiran, "Border effects, fairness, and phase transition in large wireless networks," in *Proc. IEEE INFOCOM*, 2008, pp. 601–609.

[30] K. Xu, M. Gerla, L. Qi, and Y. Shu, "TCP unfairness in ad-hoc wireless networks and neighborhood RED solution," in *Proc. ACM MOBICOM*, 2003, pp. 16–28.

[31] K. Tan, F. Jiang, Q. Zhang, and X. Shen, "Congestion control in multihop wireless networks," *IEEE Trans. Veh. Technol.*, vol. 56, no. 2, pp. 863–873, Mar. 2007.

[32] T. Rappaport, *Wireless Communications: Principles and Practice*, 2nd ed. New York: Prentice Hall, 2002.

[33] D. Couto, D. Aguayo, J. Bicket, and R. Morris, "A high-throughput path metric for multi-hop wireless routing," in *Proc. ACM MOBICOM*, 2003, pp. 134–146.

[34] A. Jindal and K. Psounis, "Achievable rate region and optimality of multi-hop wireless 802.11-scheduled network," in *Proc. Inf. Theory Appl. Workshop*, 2008.

[35] J. Padhye, S. Agarwal, V. N. Padmanabhan, L. Qiu, A. Rao, and B. Zill, "Estimation of link interference in static multi-hop wireless networks," in *Proc. IMC*, 2005, p. 28.

[36] T. Salonidis, M. Garetto, A. Saha, and E. Knightly, "Identifying high throughput paths in 802.11 mesh networks: A model-based approach," in *Proc. IEEE ICNP*, 2007, pp. 21–30.

[37] S. Rangwala, A. Jindal, K. Jang, K. Psounis, and R. Govindan, "Understanding congestion control in multi-hop wireless mesh networks," in *Proc. ACM MOBICOM*, 2008, pp. 291–302.

Apoorva Jindal (M'08) received the B.Tech. degree in electrical engineering from Indian Institute of Technology, Kanpur, India, in 1998, and is currently a Ph.D. candidate at the University of Southern California, Los Angeles.

He works on the performance analysis and design of protocols for multihop wireless networks.

Konstantinos Psounis (SM'08) received the Bachelor's degree from National Technical University of Athens, Athens, Greece, in 1997 and the M.S. and Ph.D. degrees from Stanford University, Stanford, CA, in 1999 and 2002, respectively.

He is an Assistant Professor of electrical engineering and computer science at the University of Southern California, Los Angeles. He models and analyzes the performance of a variety of networks and designs methods to solve problems related to such systems. He is the author of more than 50 research papers.

Prof. Psounis has received faculty awards from National Science Foundation, the Zumberge Foundation, and Cisco Systems.